공학석사 학위논문

Design, Analysis and Manufacturing of Variable Camber Morphing Wing with Deployable Scissor Structures

전개형 시저스 구조를 이용한 가변 캠버 모핑 날개 설계, 해석 및 제작

2021 년 2 월

서울대학교 대학원

항공우주공학과

최 이 령

Design, Analysis and Manufacturing of Variable Camber Morphing Wing with Deployable Scissor Structures

전개형 시저스 구조를 이용한 가변 캠버 모핑 날개 설계, 해석 및 제작

지도 교수 윤 군 진

이 논문을 공학석사 학위논문으로 제출함

2020 년 12 월

서울대학교 대학원

항공우주공학과

최 이 령

최이령의 공학석사 학위논문을 인준함

2020 년 12 월

위 원 장 신 상 준 (인)

부위원장 윤 군 진 (인)

위 원 김 지 환 (인)

Abstract

Design, Analysis and Manufacturing of Variable Camber Morphing Wing with Deployable Scissor Structures

Yeeryung Choi
Department of Aerospace Engineering
The Graduate School
Seoul National University

A morphing wing means a wing that changes shape. In this thesis, the morphing wing that transforms camber was designed, analyzed and manufactured among various types of shape morphing wing. The camber morphing wing is designed to satisfy airfoil shapes with a constant chord length and different cambers. The target airfoil shapes were set to four digit NACA airfoil shapes, and each rib constituting the wing was designed to implement a shape independently to perform as a twist morphing wing.

The rib constituting the camber morphing wing that is, the

internal mechanism of the rib, was newly devised, and a deployable scissor structure capable of implementing various curvatures among the deployable structures was used for the mechanism. A mathematical model was created to make the deployable scissor structure to be applied to the internal mechanism, and the shape of the internal mechanism with deployable scissor structure is determined according to the angle set as the input parameter. This mathematical model was applied to the optimum design process, and through the process the difference between the shape made by the internal mechanism and the target airfoil shapes can be reduced, thus realizing the target airfoil shapes. Since driving force is required to deform the shape of the internal mechanism, a modeling process was performed to provide connectivity between the model composed of the deployable structure and the actuator that gives the structure a driving force. When the angle for the target shape is input to the actuator, the corresponding shape is implemented. The completed model was simulated with the multibody dynamic software Recurdyn® V9R3, and it was confirmed that the target shapes were implemented very closely.

Three-dimensional modeling was performed through the above process and the analysis was conducted using multi-body dynamics software Recurdyn® V9R3. Because the structure of the camber morphing wing is deforming the shapes, the skin covering the wing must be flexible enough to be stretched according to the change in the structure's shape. The designed camber morphing wing has to have different properties depending on the direction, so a composite material was applied. Through the simulation, the behavior of the skin was analyzed.

The model designed based on the process was manufactured. The span was about 1.1m, the chord length was 0.5m, and the material was made of plywood. The manufactured wing consists of ten ribs, and one actuator operates for each rib. Therefore, each rib is driven independently to represent different shapes and target airfoil shapes.

Keywords : Morphing wing, Deployable structures, Optimal design, Camber

Student Number : 2019-26125

Table of contents

List of figures

List of tables

1. Introduction

1.1. Background and motivation

In aircraft research, it is crucial to study aircraft that can respond to various flight conditions while having high efficiency. However, there are limitations in expanding the range of operation with the existing wing of fixed shape.

Wings having fixed shapes use various devices such as ailerons, flaps, slats, and etc. to cope with the flight environment, but the advantages of using these devices are relatively limited, generally reducing efficiency by creating discontinuities in the wings. Therefore, to overcome the limitations of the existing aircraft wings, research on a morphing wing that can perform various missions in a given flight environment has been conducted. The morphing can continuously change the wing shape to increase energy efficiency and aerodynamic performance.

Morphing wing means a wing that can be changed according to the purpose, and is classified under the deformation of planform, out-of-plane, and airfoil [1]. The category of planform morphing wing

consists of morphing wing of the span, chord, and sweep. There is a lot of research on the planform morphing wing about design, analysis, and experiment[2]–[11]. Neal et al. presented a variable planform morphing wing to alter span and sweep angle with pneumatic actuators, electromechanical and lead-screw actuators [11]. Also, Perkins et al. applied advanced materials such as shape memory polymers to change the chord and augment planform area by 80 percent [2]. The out-of-plane morphing wing contains morphing wing of twist, spanwise bending, dihedral/gull. The study of out-of-plane has been designed in a various ways [12]–[15]. Majji et al. proposed a twist wing composed of ABS plastic structure and covered with an elastomeric skin [14]. Abdulrahim and Lind presented the aerodynamic and aeroelastic effects of gull morphing wing [15]. Lastly, airfoil morphing wing includes camber and thickness morphing wing. Among airfoil morphing wings, the camber morphing wing of mechanism has been studied by many methods. Also, a lot of analysis, manufacturing, and experiment were made about the variable camber morphing wing [16], [17], [26]–[28], [18]–[25]. Also, if the camber morphing wing can gradually change

the camber along the span, it can be implemented as a twist morphing wing [29]. Yokozeki et al. applied a corrugated structure to the camber morphing wing [28]. Corrugated structure in Morphing structure ranged from 69% to 90% of chord position. This section of skin is divided into upper skin(CFRP) and lower skin(thin plastic sheet) [27]. Also wind tunnel test was carried out by the camber morphing wing with corrugated structures[24], [27]. Joo et al. designed VCCW(Variable Camber Compliant Wing) based on compliant mechanisms [22]. They set six target airfoil shapes (NACA 2410 – NACA 8410) with only camber difference while maintaining maximum camber location and maximum thickness the same [22], [23]. The skin of VCCW is seamless, continuous, and made with non-stretchable composite. Christopher et al. conducted wind tunnel testing of the Variable Camber Compliant Wing. Also, they measured surface displacement (the deformation of the wing) by 3D digital image correlation [23].

1.2. Objectives and Overview

In this thesis, a morphing wing that changes camber was designed and manufactured. Camber refers to the distance between the average camber line of the airfoil and the chord line, that is, an airfoil's curvature. The camber morphing wing's goal is to alter the camber uniformly along the span, so that the wing can be morphed more continuously than using devices (flaps, slats, ailerons, etc.) on a wing having the fixed shape. It has to be carried out as a controllable twist morphing wing by gradually changing the camber along the span.

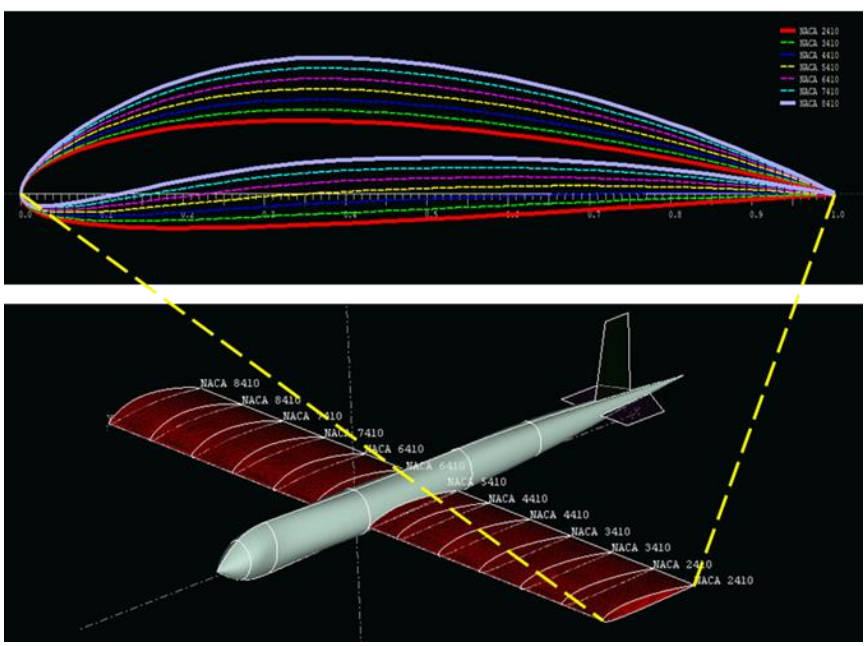

Figure 1. Camber morphing wing (XFLR5)

The design goal of the camber morphing wing was set to alter only the camber without changing the chord length. Also, each of the ribs constituting the wing must be able to form various airfoil shapes independently. The chord length was set to have a constant value during the deformation, and the target airfoils to be performed were set in seven NACA airfoils (NACA2410, NACA3410, NACA4410, NACA5410, NACA6410, NACA7410, NACA8410). Accordingly, a novel mechanism was devised and designed to accurately implement various airfoils while being efficient in transforming the camber, and this design model was analyzed and manufactured. The internal mechanism of the camber morphing wing presented in this thesis is simple. It is composed of an uncomplicated structure and allows camber to be changed to realize the exact shapes. The internal mechanism is applied to the wing's ribs, so that each rib can deform shape independently. The dimensions of the deployable structure are obtained through mathematical modeling and optimization. This mathematical modeling and optimization process can also be applied to implement other airfoils. Through this process, it is possible to minimize the shape differences between the target airfoil shapes.

Three-dimensional modeling was performed through the above process and the analysis was conducted using multi-body dynamic software Recurdyn® V9R3. The structure of the camber morphing wing is altering the shapes, so the skin covering the wing must be flexible enough to be stretched according to the change in the structure's shape. Thus, the skin is required to have low in-plane stiffness and high out-of-plane stiffness [30]. Besides, the designed camber morphing wing should not be stretched in the spanwise direction but must stretch the most in the chordwise direction. Therefore, a composite material was applied to the skin. Through the simulation, it was possible to determine which part of the skin has maximum stress and strain while the camber is changing.

The wing was manufactured based on three-dimensional modeling from the design. The chord length was manufactured with the target length of 500mm, but the span was manufactured about 65% of the designed reference span. There are ten ribs to which the internal structure is applied, and an actuator is inserted for each rib.

2. Camber Morphing wing with Deployable structure

2.1. Deployable Structure

Deployable structures are the structures that can be folded and unfolded by hinged nodes of the structure. Thus, they have the characteristics of varying shape and volume and are classified according to the structural system. Deployable structures can transform a variety of configurations and deform in known ways [31]. These abilities of deployable structures can make being able to be applied to the diverse fields [32]–[35]. Deployable structures are classified under spatial bar structures consisting of hinged bars, foldable plate structures consisting of hinged plates, tensegrity structures, and membrane structures [32]. Among these, a deployable scissor structure was applied to the camber morphing wing.

Deployable scissor structure is very versatile. The structure is deployable in scissors and can be configured as a structure that resists load after deployable [36]–[38]. The structure consists of straight bars and a revolute joint and can be deployable using the

joint at the center. The straight bars and joints rotate relative to each other, and the structure deploys and retracts.

To deploy a scissor structure, one constraint must be satisfied, which is called a deployability constraint [32]. The deployability constraint is the formula for the length that forms the deployable scissor structure. As shown in Figure 2, The structure can be deployable when the lengths of the square formed by the scissors satisfy Eq (1).

$$a_0 + b_0 = c_0 + d_0 \tag{1}$$

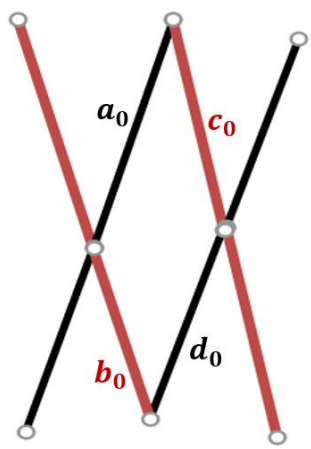

Figure 2. Deployability constraint

Unit of the deployable scissor structure consists of a revolute joint and two straight bars intersect by the joint. The shape of structure varies depending on the geometries such as units' length and angle. Thus, the shape of the morphing wing is determined according to the dimension of the unit. Since the deployable scissor structure can perform various curvatures, it is appropriate to form the airfoil shape [39]–[41].

2.2. Internal Mechanism with Deployable Structure

Representative methods of changing the camber are using an internal mechanism, piezoelectric actuation, and shape memory alloy actuation [29]. In this thesis, it is designed in a way that alters the camber using an internal mechanism.

The internal mechanism of the camber morphing wing was applied with the deployable scissor structure. To deform the camber, the internal mechanism to be applied to the rib was devised for concept design as shown in Figure 3.

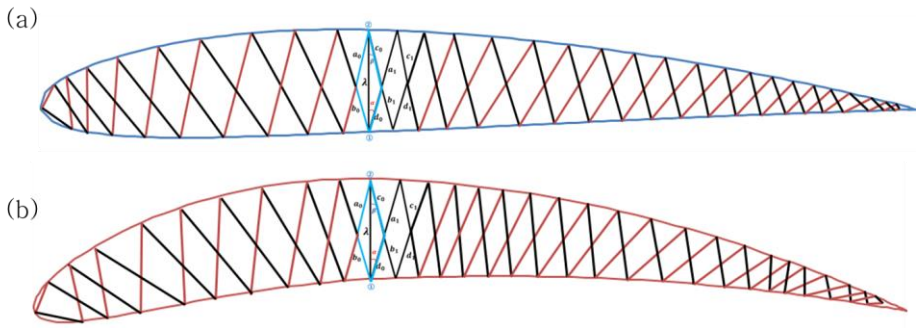

Figure 3. Concept design of camber morphing wing rib with Deployable structure

Deployable scissor structure increases the volume and cross-sectional area occupied by the structure as it deploys. As the number of scissor units constituting the structure increases, the difference between the volume and cross-sectional area before and after deployment increases. One of the design goals for the camber morphing wing is the condition that the chord length must be kept constant during the deformation. If the number of scissor units is exceeded, the internal mechanism's chord length will become longer as the structure deploys. Thus, the number of scissor units must be set so that the airfoil's chord length can be kept almost constant, while the camber of the airfoil can achieve the target curvature.

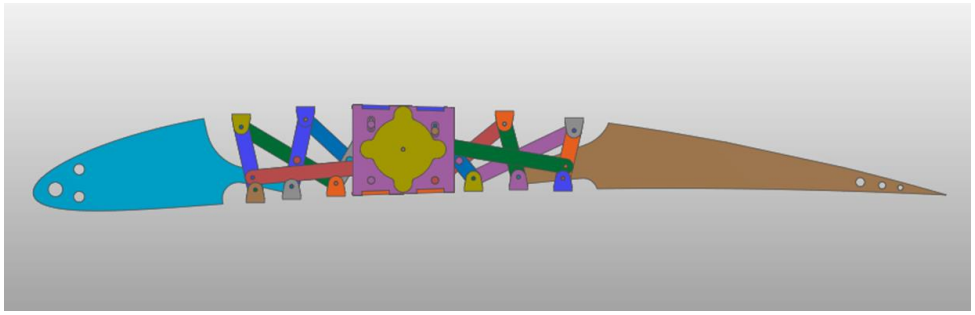

Figure 4. Developed design of camber morphing rib with the deployable structure

To improve the durability and operability of the structure, the design was developed as shown in Figure 4. The design composition is classified into deployable scissor structure, fixed shape part, connection part, and actuator. The components consisting of the deployable scissor structure that can alter the structure's whole shape are shown in Figure 5.

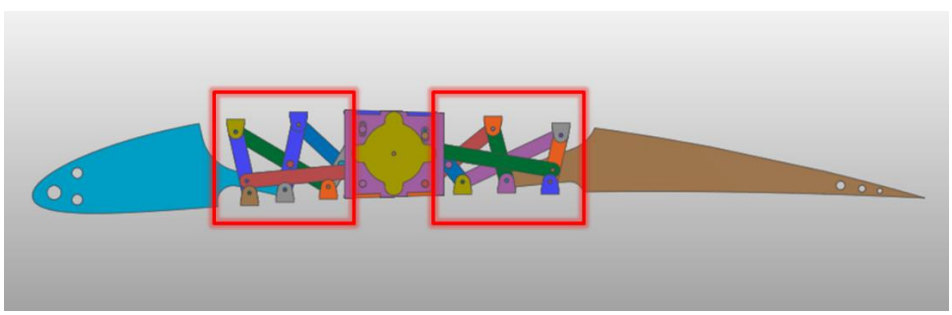

Figure 5. Deployable scissor structure of camber morphing wing rib

In the deployable scissor structure part, one member in Figure (a) is connected to the two members shown in Figure 6. Figure 6(c) by a revolute joint each. These are connected back and forth in a symmetrical way. Figure 6 (b) and (d) show the marked members in Figure 6 (a) and (c) from different directions for each.

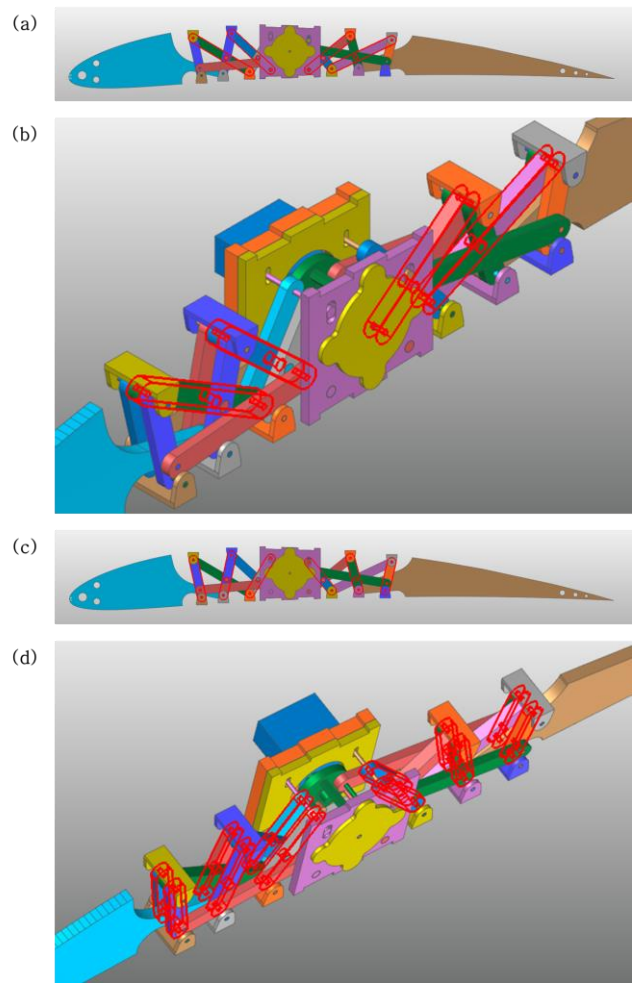

Figure 6. Components of Deployable scissor structure

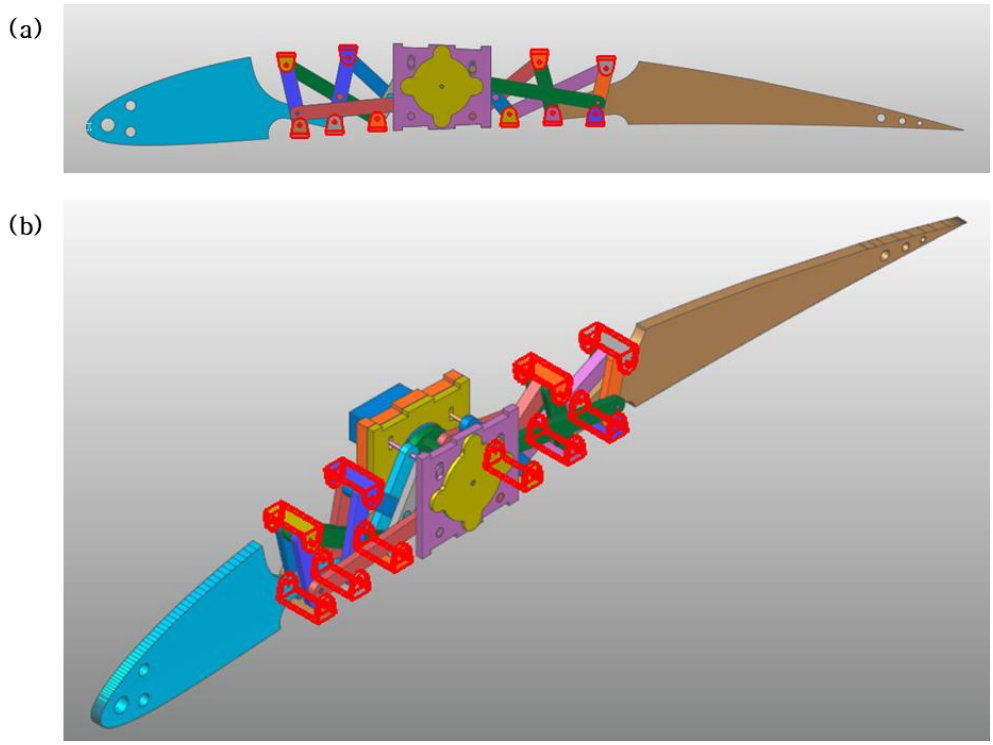

Figure 7. Offset parts with Deployable scissor structure

Figure 7 shows the offset parts attached to the deployable scissor structure. Offset parts function as making the adhesive surface for the skin to be covered on the morphing wing. The offset parts are connected with the members by a revolute joint and can be rotated using this connection position as an axis of rotation. Additionally, there is some friction between offset parts and the members.

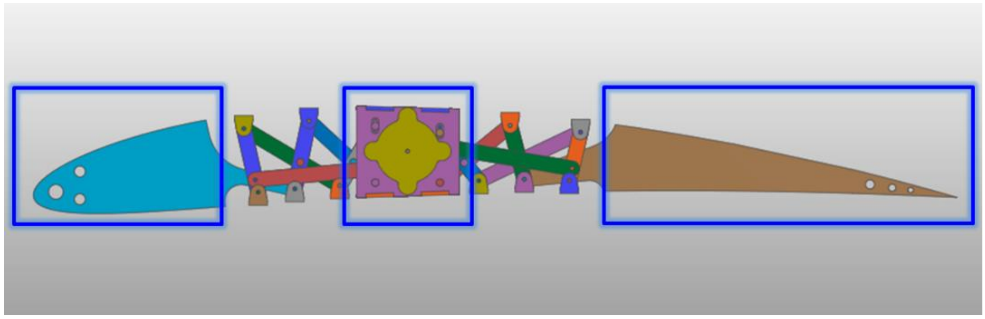

Figure 8. Fixed shape parts of camber morphing wing rib

The parts marked in Figure 8 are the fixed-shape parts, which consist of the leading edge part, trailing edge part, and spar part with an actuator attached to it. The actuator attached to the spar allows the structure to move by applying a driving force. Since the structure is designed to have one degree of freedom, the degree of freedom is controlled by an actuator. As the degree of freedom, an angle related to the actuator and the deployable structure parts is specified. This angle corresponding to the target shape is input by the actuator. All target airfoils have a common feature the maximum camber position is 40% of the chord length from the leading edge. In the fixed-shape parts structure, these were designed based on NACA 5410 having an intermediate camber value among the target airfoil shapes. Except for the spar, the parts with the fixed shaped structures are connected

to the deployable structure and move according to the deployable structure's movement. In the group of these, the spar does not move. The spar was positioned based on the coordinates common to the target airfoils. Moreover, these coordinates are close to the maximum camber position.

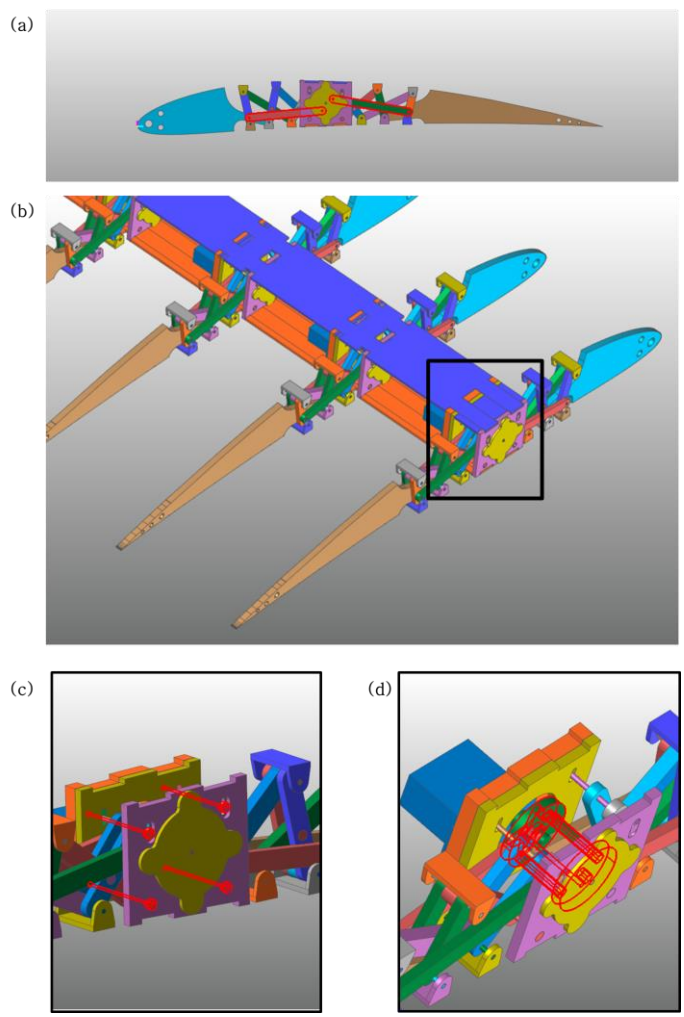

Figure 9. Connection components of camber morphing wing rib

The parts in Figure 9(a), (c), and (d) belong to the connection part. The connection part comprises members that connect the deployable structure and the fixed shape part, and members transmit the driving force of the actuator to the structure. The elements marked in Figure 9(a) and (d) connect the actuator and the deployable structure part. These members deliver the torque that the actuator generated so that the deployable structure can get movement. The connection parts indicated in Figure 9(c) are the bars connecting the deployable structure and the spar. Two bars at the top move only vertically and two bars at the bottom are fixed to the spar without movement.

The ribs were designed according to the method described, and these ribs constitute the camber morphing wing. Since the ribs can independently form various airfoil shapes, they can also perform as a twist morphing wing.

3. Design of Camber Morphing Wing

3.1. Modeling of the Wing Rib with Deployable Structure

3.1.1. Mathematical Modeling of the Internal Mechanism

To generate the airfoil with the internal mechanism, a mathematical model of the dimension constituting the internal mechanism that decides the shape of the structure is required. In deployable structure, because the length of the members and the connection angle determine the structure's shape, the mathematical model is created for the length and angle. The mathematical model can find the optimal value of lengths for the angle when the angle is given as input value. Therefore, it is possible to calculate the shape produced by the internal mechanism. The input angle is set to the degrees of freedom for the entire structure. Also, it can calculate the difference between the shape generated and the actual airfoil that we targeted.

To be applied to the deployable scissor structure, the deployability constraint (Eq (1)) must be satisfied. Mathematical modeling proceeds with dimensions that satisfy this constraint.

Based on the spar's position, the deployable scissor structures are designed the same for the leading edge and trailing edge sides and consist of three scissor units on each side. The same mathematical model is applied to both sides, and the deployable scissor structure connected to the right section is addressed for the first step of the mathematical modeling. Additionally, the chordwise direction was set to the x−coordinate direction, the spanwise direction was set to the z−coordinate direction and the direction perpendicular to these directions was set to the y−coordinate direction.

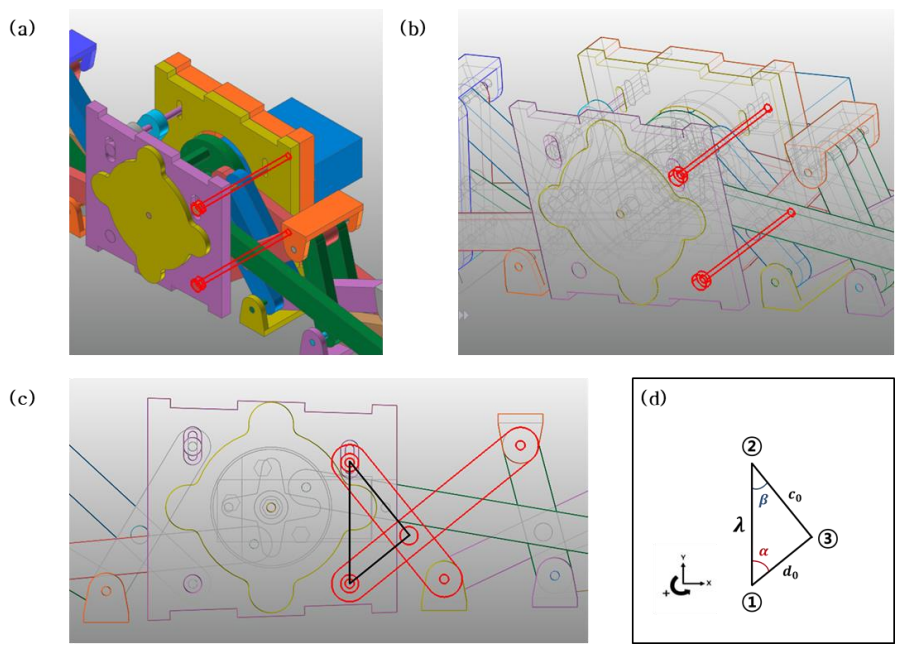

Figure 10. Connection part for deployable scissor structure and spar

Figure 10(a) and (b) show two bars connected to the deployable structure parts using revolute joints. Figure 10(c) represents the cross-section, and the dimensions of the triangle shown are defined as in Figure 10(d). In Figure 10(d), Point ① is the bar's coordinate at its fixed location without movement. Point ② is the coordinate of the bar located at the top that only moves up and down. Point ① and point ② are set as having a same x-coordinate value. The length of the line connecting point ① and point ② is set to λ. Point ③ in the triangle in Figure 10 (d) is the coordinate of the first unit's revolute joint in the right section. And the length between point ② and point ③ is set as c_0 and the length between point ① and point ③ is set as d_0. α and β are the angles that make up the triangle. Given the lengths of all three sides of the triangle, the angles of the triangle can be founded by using the second law of cosines. Thus, angles can be expressed in terms of side lengths in Eq (2) and (3).

$$\alpha = cos^{-1}\left(\frac{\lambda^2 + {d_0}^2 - {c_0}^2}{2\lambda d_0}\right) \qquad (2)$$

$$\beta = cos^{-1}\left(\frac{\lambda^2 + {c_0}^2 - {d_0}^2}{2\lambda c_0}\right) \quad (3)$$

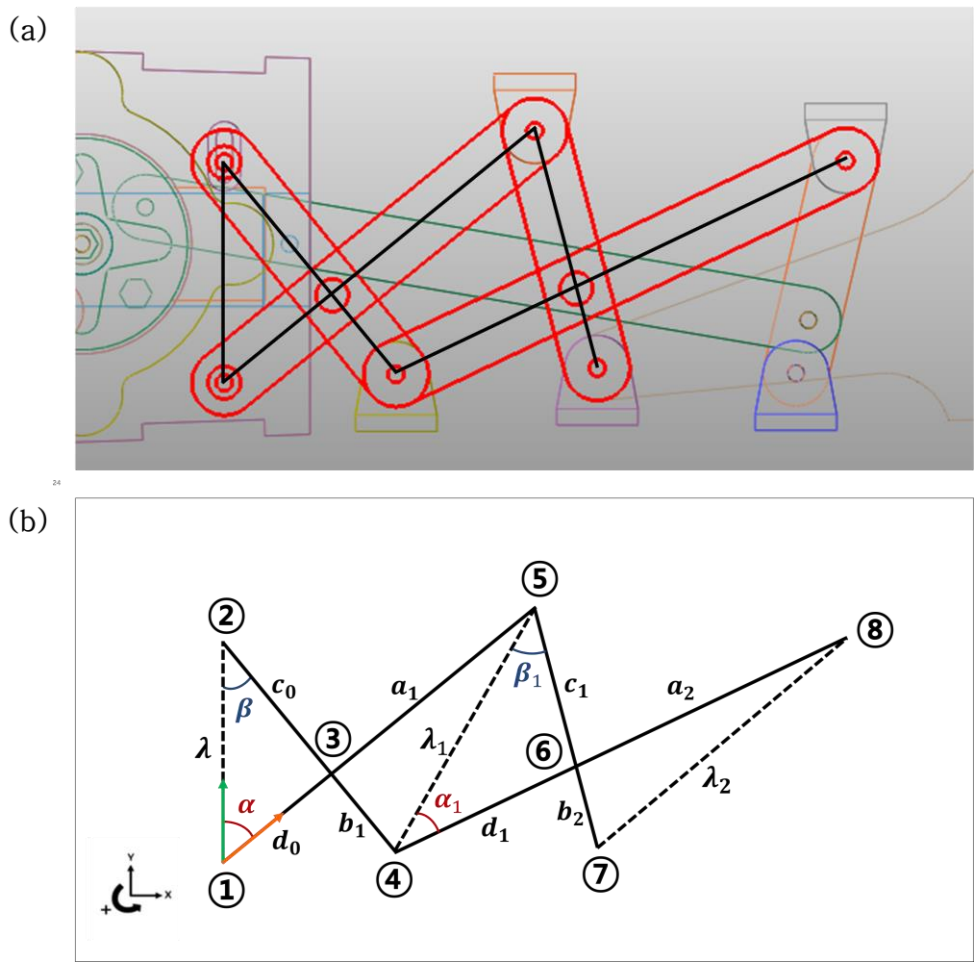

Figure 11. Deployable scissor structure right section and dimension

Figure 11 displays more areas than those shown in Figure 10. Using the coordinates and dimensions at point ①, point ② and point ③, the

coordinates and dimensions of other points can be obtained. Since the straight line connecting point ① and point ② is vertical, the unit vector from point ① to point ② is (0,1,0). If the unit vector is rotated clockwise by the angle α, the unit vector from point ① to point ③ can be derived. The process is shown in Eq (4), (5), (6) and (7).

$$vector_{1-2} = \begin{bmatrix} x_2 \\ y_2 \\ z_2 \end{bmatrix} - \begin{bmatrix} x_1 \\ y_1 \\ z_1 \end{bmatrix} \tag{4}$$

$$unitvector_{1-2} = \frac{vector_{1-2}}{\sqrt{(x_2-x_1)^2+(y_2-y_1)^2+(z_2-z_1)^2}} = \begin{bmatrix} 0 \\ 1 \\ 0 \end{bmatrix} \tag{5}$$

$$\mathrm{A_{rotation}} = \begin{bmatrix} \cos(-\alpha) & -\sin(-\alpha) & 0 \\ \sin(-\alpha) & \cos(-\alpha) & 0 \\ 0 & 0 & 1 \end{bmatrix} \tag{6}$$

$$vector_{1-3} = d_0 * A_{rotation} * unitvector_{1-2} \tag{7}$$

$$vector_{1-5} = (d_0 + a_1) * A_{rotation} * unitvector_{1-2} \tag{8}$$

The unit vector from point ① to point ③ is the same as the unit vector from point ① to point ⑤. And since the distance between point ① and point ⑤ is $(a_1 + d_0)$, the vector from point ① to point ⑤ and coordinate of point ⑤ can be obtained as Eq (8).

$$vector_{2-1} = \begin{bmatrix} x_1 \\ y_1 \\ z_1 \end{bmatrix} - \begin{bmatrix} x_2 \\ y_2 \\ z_2 \end{bmatrix} \tag{9}$$

$$unitvector_{2-1} = \frac{vector_{1-2}}{\sqrt{(x_2-x_1)^2+(y_2-y_1)^2+(z_2-z_1)^2}} = \begin{bmatrix} 0 \\ -1 \\ 0 \end{bmatrix} \tag{10}$$

$$B_{\text{rotation}} = \begin{bmatrix} \cos(\beta) & -\sin(\beta) & 0 \\ \sin(\beta) & \cos(\beta) & 0 \\ 0 & 0 & 1 \end{bmatrix} \tag{11}$$

$$vector_{2-4} = (c_0 + b_1) * B_{rotation} * unitvector_{2-1} \tag{12}$$

Through a similar process, Eq (9), (10), (11), and (12) can be induced. As a result, the vector from point ② to point ④ and coordinates of point ④ can be gained. Since the coordinates of point ④ and point ⑤ and the distance between the points λ_1 can be obtainable by the coordinates, the angles and the lengths of the

triangle consisting of point ④, point ⑤, and point ⑥. Finally, if the calculation is repeated, all the deployable scissor structure coordinates can be known.

3.1.2. Actuation Modeling with the Internal Mechanism

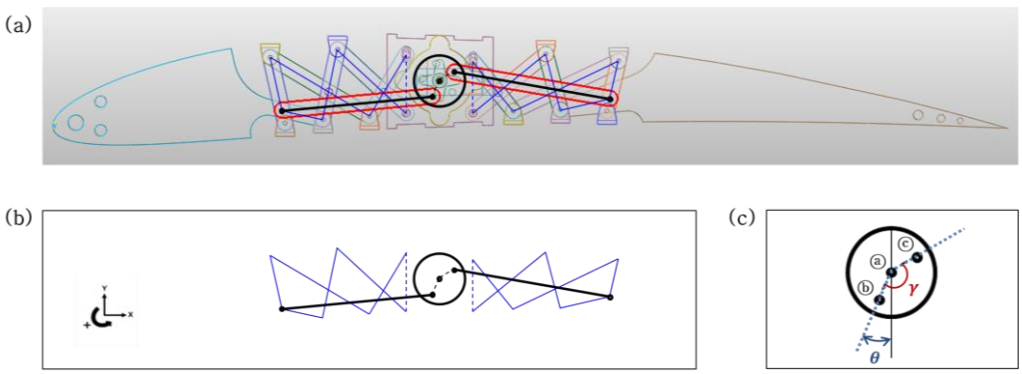

Figure 12. Connection part between the actuator and the deployable structure part

The deployable scissor structure needs the power to deploy. Therefore, a rotary actuator and the structure were connected and the force was transmitted. Figure 12(a) and (b) show the connection between the structure and the actuator. According to the design condition, it is composed of three scissor units of deployable structure on both sides based on the spar. Also, the position of the

revolute joint for the third scissor unit connected to the fixed shape structure can be known by the mathematical model. Moreover, a link has been installed that connects the revolute joint and the actuator to transmit the driving force.

The entire structure is moved by one actuator, fixed to the disk shown in Figure 12(c). The disc is coupled with the leading edge and trailing edge by two links each and has a center as Point ⓐ. These links connect to two holes drilled in the disk, marked in Figure 12(c) as Point ⓑ and Point ⓒ. γ is the angle between two links and this angle has a fixed value. In contrast, the angle θ is a changing value. θ is the angle between the vertical line passing through Point ⓐ and the link connecting to the leading edge. Moreover, when the members' lengths are fixed, the angle θ was configured as an input parameter that determines the shape of the structure. Therefore, by changing the value of this parameter, the airfoil of the camber is altered.

3.2. Optimum Design of Internal Mechanism with Deployable structure

The camber morphing wing of the internal mechanism must be designed to fit the shape of the airfoil accurately. Since there are seven target airfoils to be implemented, it is not easy to generate all of them accurately if the dimensions of the scissor structure are arbitrarily set. In other words, there are differences between the target airfoils and the shape made by the internal mechanism. Therefore, an optimization process was conducted to reduce the differences. The optimization process is designed to minimize the distances between the target airfoil coordinates and the airfoil coordinates. In the optimization, the parameter to consider is the angle θ in Figure 12(c), which is the given parameter for each target airfoil. The angles are fixed values and entered into the actuator. In other words, it is necessary to obtain the lengths of the scissor members so that the internal mechanism, which varies according to the angles, can be implemented without error as much as possible for the seven target airfoils. Table 1 shows the values of angles to implement each target airfoil.

Table 1. Set angle θ for target airfoils

Airfoil / Parameter	NACA 2410	NACA 3410	NACA 4410	NACA 5410	NACA 6410	NACA 7410	NACA 8410
Angle θ	7°	13°	19°	25°	31°	39°	49°

The coordinates of the airfoil generated by the internal mechanism will be referred to as the deployable scissor structure's coordinates. First, a standard for matching the target airfoil coordinates and the coordinates of the deployable scissor structure to each other is required. Since the target airfoils are all four digit NACA airfoils, two million points per airfoil were calculated using the formula for four digit NACA airfoil. The coordinates created by members of the deployable scissor structure can be obtained through the mathematical model. However, since the airfoil-shaped surface is implemented by the offset parts attached to the deployable scissor structure, the offset parts represented in Figure 7 must also be considered. Because the offset parts can be rotated, the coordinate where the offset parts are in contact with the skin must be found. After the progress, the coordinates can be matched with the target

airfoil coordinates. The angles between the offset parts and scissor members are selected as the most suitable value using four cases. The offset part in Figure 13(a) will be explained as an example. One offset part is connected to two scissor members. In Figure 13(b) and (c), the offset parts have the directions that the two connected scissor members are indicated.

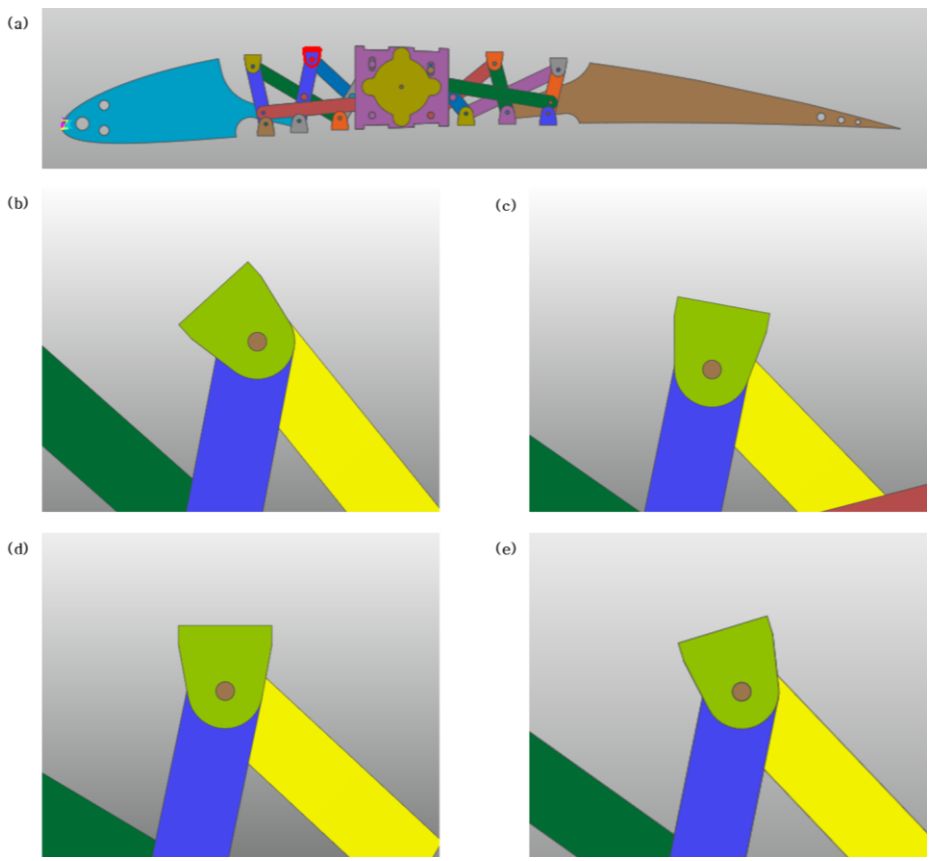

Figure 13. Directions of Offset part

In using the offset part in Figure 13(d), the skin is supported vertically. Lastly, as shown in Figure 13(e), the offset part has a diagonal direction passing through the rotational center of the offset part in the quadrangle generated by the connection of the scissor units. In these four cases, the point of the coordinate $[x_{sc}, y_{sc}, z_{sc}]_m$ $(\mathrm{m} = 1,2,\ldots)$ where the offset part attaches to the skin can be obtained. Among the two million points on the target airfoil curve obtained earlier, one of the points that match the offset part's coordinate can be set through the standard. First, to explain the standard, the point$[x_{ra}, y_{ra}, z_{ra}]_m$ $(\mathrm{m} = 1,2,\ldots)$ is defined as the target airfoil coordinate. And, if the x−coordinate of this point(x_{ra}) has the closest value to the x−coordinate of the offset part(x_{sc}), then two points correspond to each other. Here, the coordinates where the offset part touches the skin is the same as the coordinates of the scissor structure defined above.

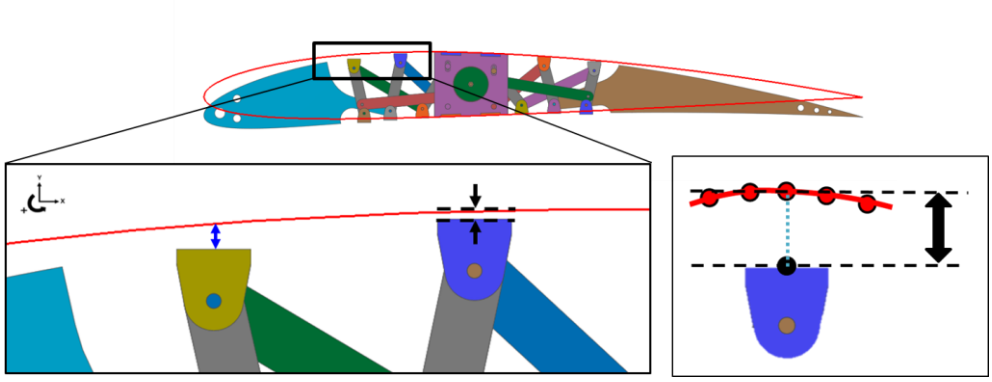

Figure 14. Distance between the offset part and desired airfoil

$$d_m = \sqrt{(x_{ra} - x_{sc})_m{}^2 + (y_{ra} - y_{sc})_m{}^2 + (z_{ra} - z_{sc})_m{}^2} \qquad (13)$$

$$(m = 1,2,3, \dots)$$

$$S_{Airfoil} = \sum_{m=1}^{n} d_m \qquad (n = 1,2,3, \dots) \qquad (14)$$

$$T_{target\ airfoils} = \sum_{n=2}^{8} S_{n410} \qquad (15)$$

The distance between the corresponding points can be represented as Eq (13). Through Eq (14), the shape difference for one airfoil can be calculated by summating all the differences between the point on the target airfoil and the offset part. So, using Eq (15), the sum of the seven target airfoil shape differences ($T_{target\ airfoils}$) can be

gained by adding all the differences per airfoil. Therefore, it is possible to get parameter values that minimize the sum of all the differences between the actual airfoil shape and the airfoil shape realized by the structure. The parameter values are lengths of the deployable scissor structure when input angles have the fixed values for each target airfoil.

Therefore, optimal design's input values are the lengths of the scissor members, and the values of lengths are entered with arbitrary values. Finally, through the optimum design process, output that minimizes the shape differences can be obtained.

3.3. Results for the Optimum Design

The optimal design process was calculated through Matlab®, and the results were obtained. In other words, the values of the deployable structure members that implement target airfoils can be attained. Figure 15. is a graph showing the process of optimizing the values summed for all target shapes by calculating the difference between the target airfoil coordinates and the scissor structure's coordinates according to the previously set criteria. In Figure 15., the vertical axis represents the sum of differences for all target airfoils, and the horizontal axis represents the number of repetitions.

The internal mechanism's behavior was realized by modeling the internal mechanism and applying the parameters obtained from the optimization result. Furthermore, the shape of the target airfoils was visually confirmed by the following figures.

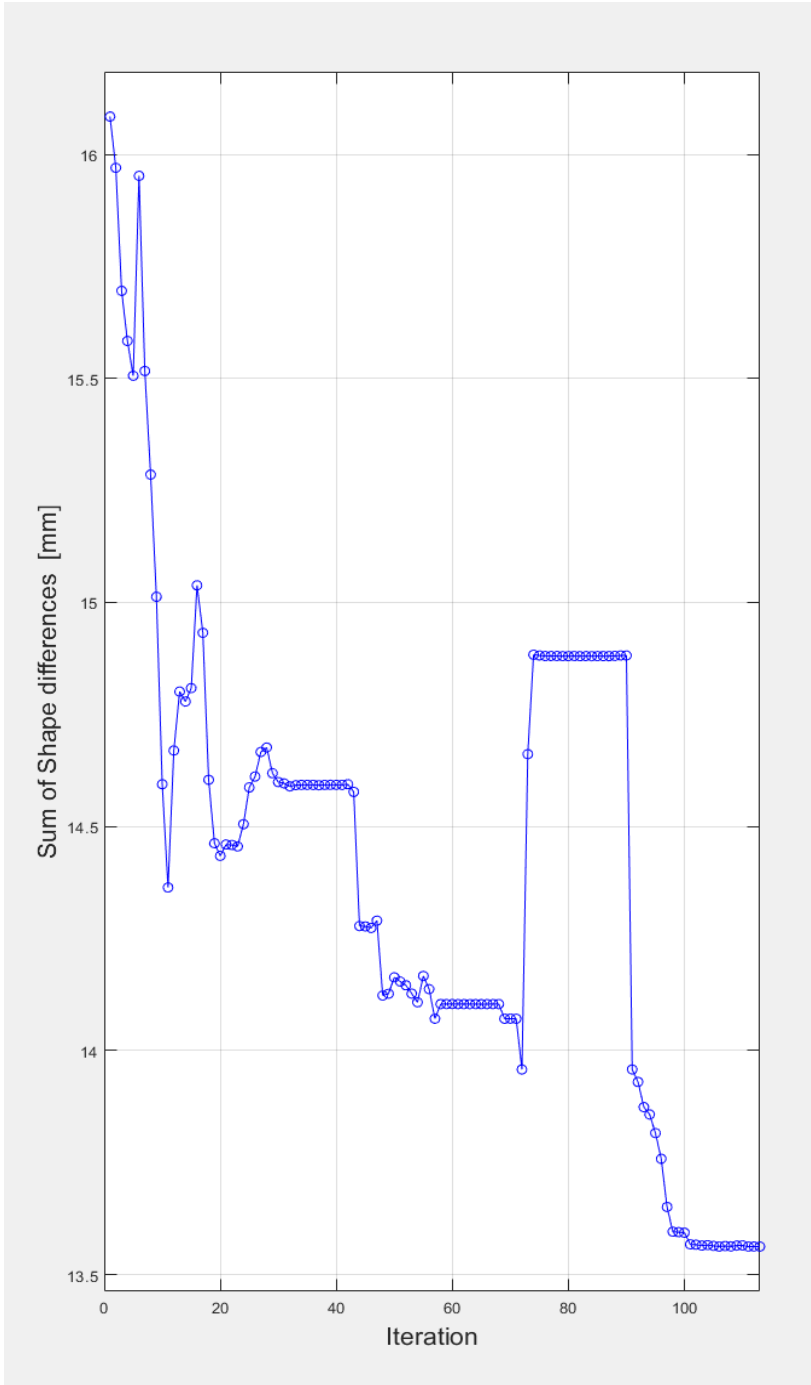

Figure 15. The optimization process of the Shape Differences

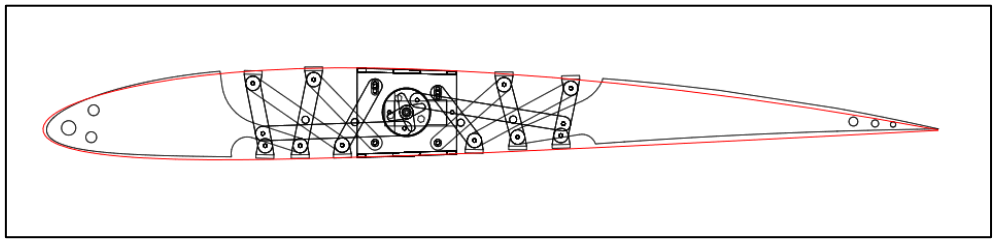

Figure 16. The shape differences between NACA 2410 and Camber Morphing Wing

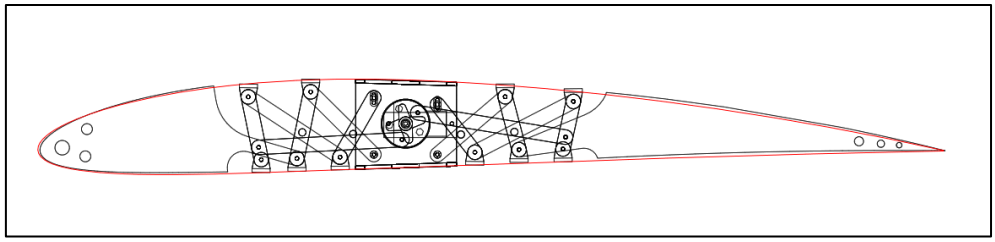

Figure 17. The shape differences between NACA 3410 and Camber Morphing Wing

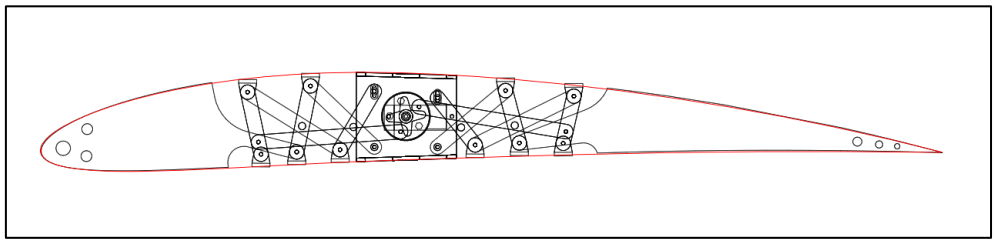

Figure 18. The shape differences between NACA 4410 and Camber Morphing Wing

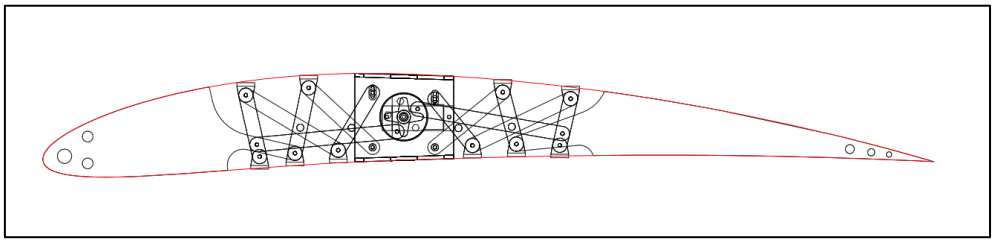

Figure 19. The shape differences between NACA 5410 and Camber Morphing Wing

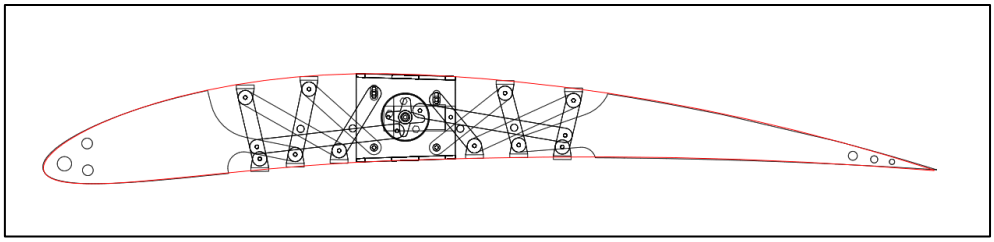

Figure 20. The shape differences between NACA 6410 and Camber Morphing Wing

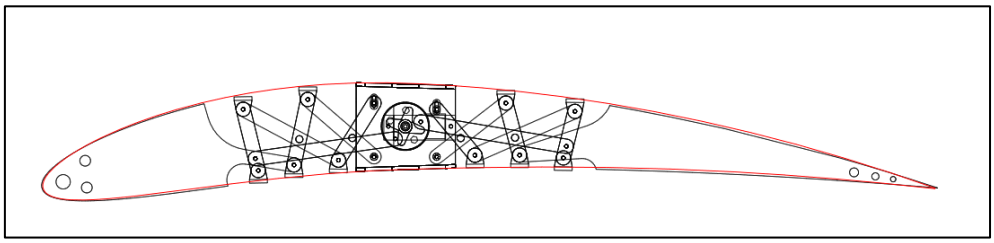

Figure 21. The shape differences between NACA 7410 and Camber Morphing Wing

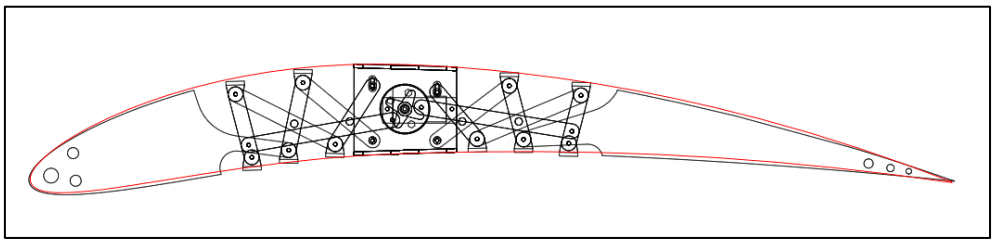

Figure 22. The shape differences between NACA 8410 and Camber Morphing Wing

The red line in Figure 16, Figure 17, Figure 18, Figure 19Figure 20, Figure 21 and Figure 22 is the target airfoil, and how close to the target shape can be checked through these figures.

The design condition had the requirement that only the camber had to be altered while the chord length remained the same. It can be seen in Figure 23 and Figure 24 that the internal mechanism satisfies this condition. The chord length is not perfectly identical. However, the chord length value from the internal mechanism is considered identical during the deformation because it has a value within a maximum of 1% the design chord length. The green line in Figure 23 is the shape of the airfoil of NACA 2410, the red line is NACA 5410, and the blue line is NACA 8410. These shapes are all airfoils with the identical chord length. Figure 24 shows that the design condition

is satisfied for all target airfoil geometries and the wing can be performed as a twist morphing wing.

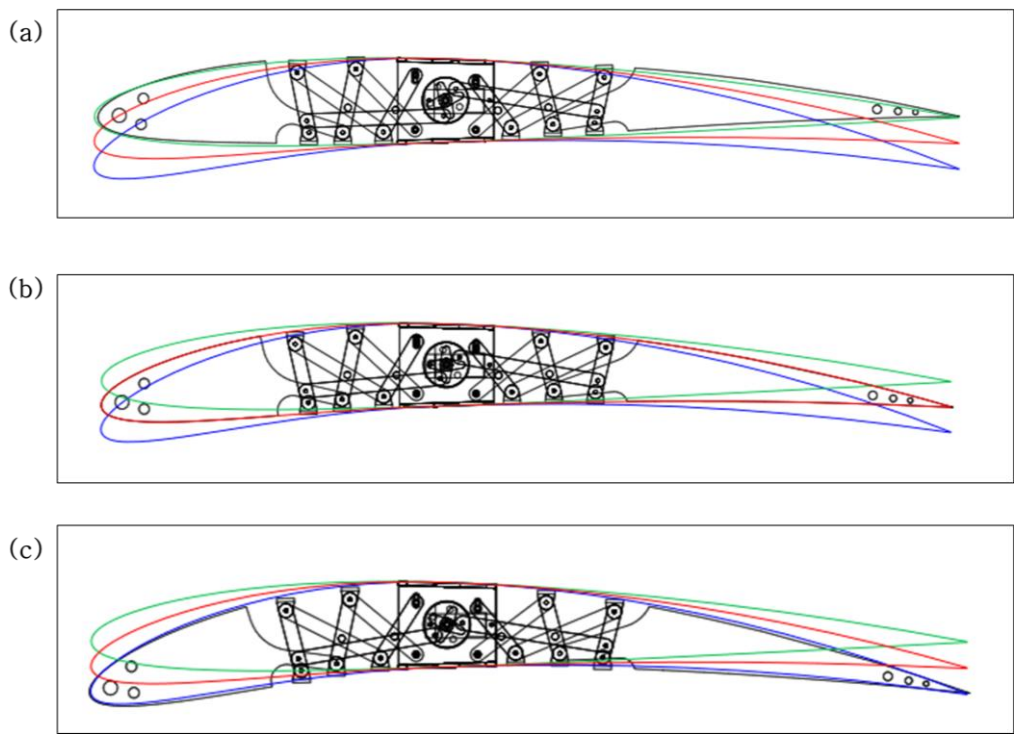

Figure 23. Comparison between the shape created by the Camber Morphing wing rib and the target shapes

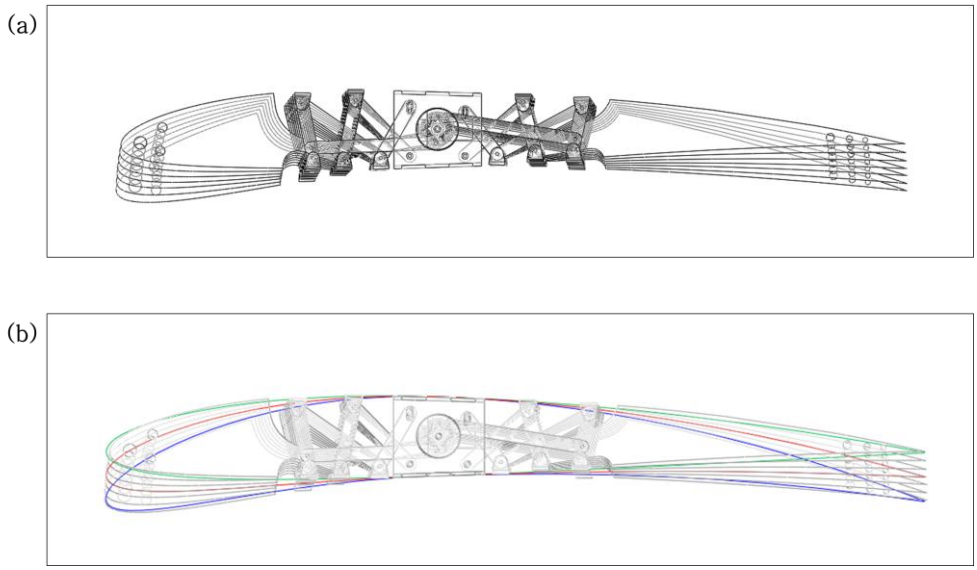

Figure 24. Deformed Camber Morphing wing as a Twist Morphing Wing

3.4. Modeling and Simulation of the Wing

Modeling was performed on the entire wing consisting of designed ribs. The wing is designed to contain 15 ribs, and the chord length is set to 0.5m. The gap between the ribs is 85mm, and the thickness per rib is 37.8mm. Thus, the total span is 1757mm. One actuator is attached to each rib, and the motor protrudes out of the rib. The rib thickness is the distance excluding the protruding part.

The rib connected to the fuselage is marked in Figure 25(a)and (b). To prevent the actuator from protruding out of the wing. Only the rib closest to the fuselage was installed in reverse as shown in Figure 25 (c). In Figure 26, the modeling of ten ribs that are part of the wing is shown.

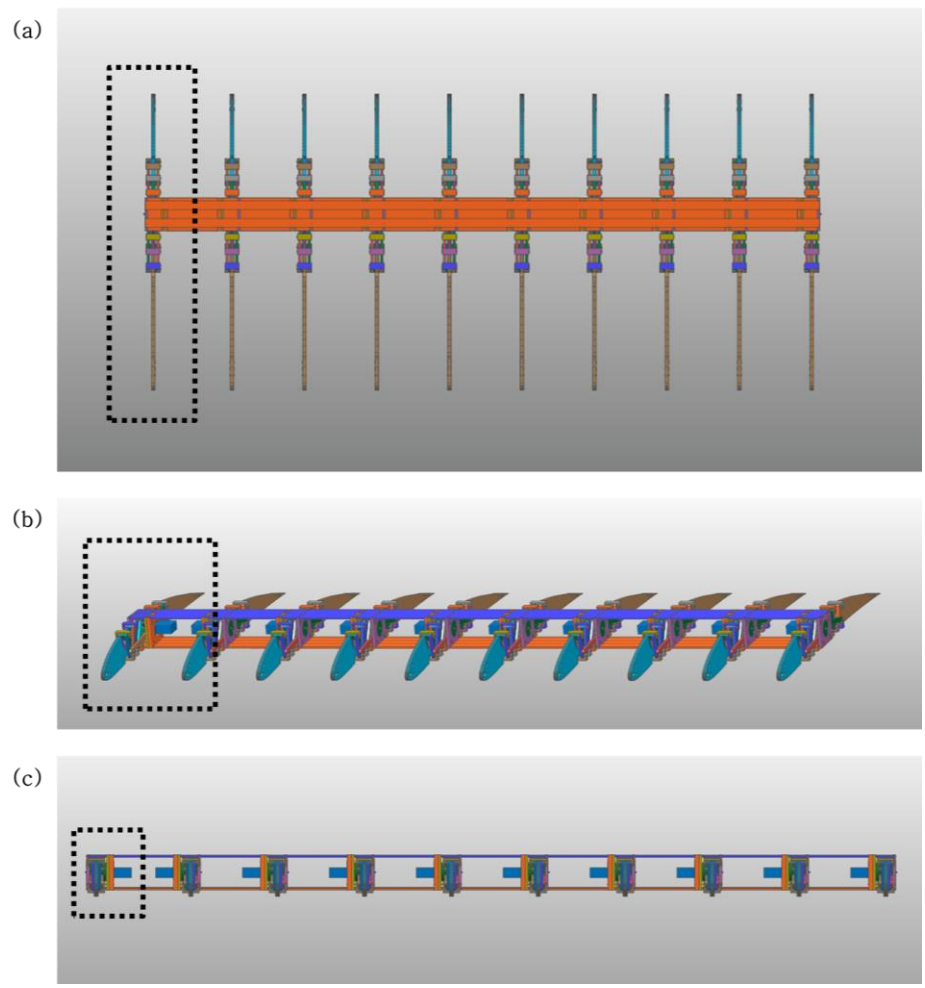

Figure 25. The rib connected to the fuselage

(a)

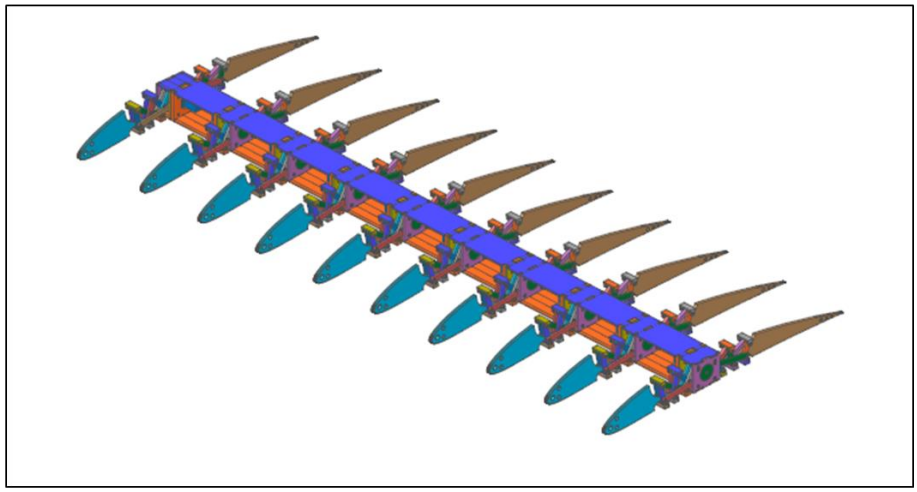

(b)

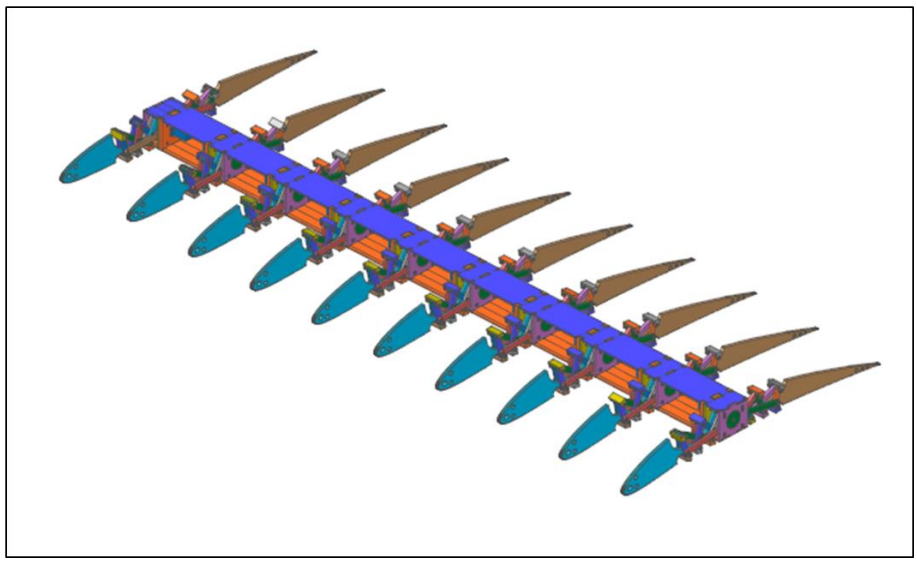

Figure 26, Modeling and Simulation of Camber Morphing Wing with ten ribs

4. Analysis of Camber Morphing Wing Skin

4.1. Camber Morphing Wing Skin

The camber morphing wing structure proposed in this thesis deforms and changes the entire shape. Therefore, the skin covering this structure must be flexible enough to deform together as the structure shape changes. At the same time, however, it is required to be rigid enough to withstand the aerodynamic force applied to the wing. In other words, the morphing wing skin has the requirements of low in-plane and high out-of-plane stiffnesses [30]. The designed model should stretch the most in the chordwise direction, not in the spanwise direction. Thus, the composite material that can have different properties depending on the direction was applied. In other words, the spanwise direction, which should have high rigidity, is set as the fiber direction.

4.2. Analysis of the Wing Skin

The analysis was performed by assuming that the composite's fiber to be applied to the skin is carbon fiber and the matrix is silicone.

The density of the carbon fiber is 1.81$\mathrm{kg/mm^2}$, the Poisson's ratio(ν_f) is 0.27, and the elastic modulus (E_f) is set as 242GPa. The specific volume of the matrix silicone is 23.5 $\mathrm{in^3/lb}$, and the Poisson's ratio(ν_m) is set as 0.485. As assuming the shore hardness of the silicone is 30A, the elastic modulus(E_m) was calculated using Eq (16) [42]. Furthermore, the shear moduli were obtained using Eq (17) from the elastic moduli and the Poisson's ratios [43]. In the composite, the volume fraction of the fiber(V_f) is assumed to be 0.6 and the volume fraction of the matrix(V_m) is 0.4.

$$logE_m = 0.00235S - 0.6403 \tag{16}$$

$$S = Shore\ A \qquad (20A < S < 80A)$$

$$G = \frac{E}{2(1+\nu)} \tag{17}$$

The properties of the composite set through this process are calculated using several formulas. First, the elastic modulus of spanwise direction (E_1) and chordwise direction (E_2) are obtained using the rule of mixture as represented in Eq (18) and Eq (19) [43].

The Poisson's ratio(ν) of the composite was obtained using Eq (20) and the density(ρ) using Eq (21) [43].

$$E_1 = \mathrm{E_f} V_f + E_m V_m \tag{18}$$

$$E_2 = \frac{1}{\frac{V_f}{E_f} + \frac{V_m}{E_m}} \tag{19}$$

$$\nu = V_\mathrm{f} \nu_f + V_m \nu_m \tag{20}$$

$$\rho = V_\mathrm{f} \rho_f + V_m \rho_m \tag{21}$$

The skin properties were determined through Eq. (18), (19), (20), and (21), and the model was made for a wing consisting of seven rib. The analysis was performed using the multibody dynamic software Recurdyn® V9R3. The skin is set as an isotropic material using the chordwise direction of the elastic modulus. All of the initial morphing wing ribs form the NACA 5410. In Figure 27 , the analysis model of skin is represented.

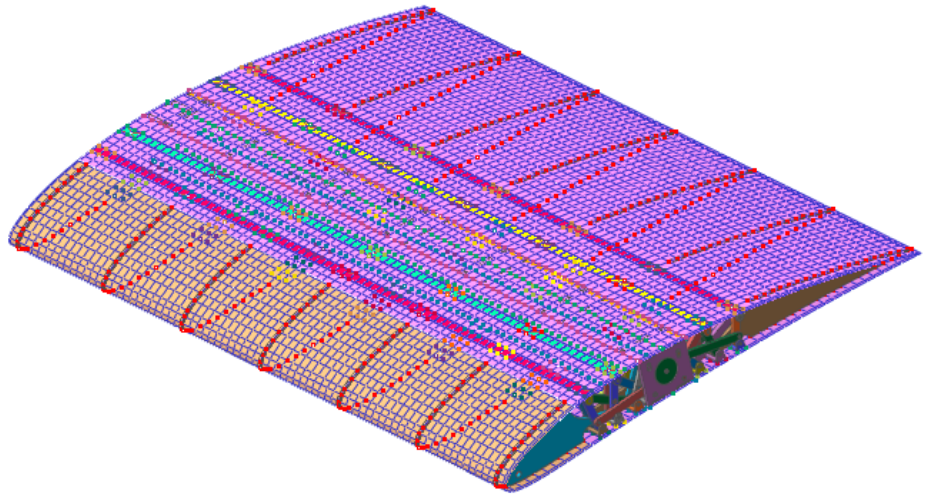

Figure 27. Analysis of Camber Morphing Wing Skin

The mesh type of skin is composed of shell4 quad4 elements, and the mesh size is 10, which is mostly the same size, but the leading edge part with large curvature is divided into smaller meshes.

The spar's side attached to the aircraft fuselage is fixed. The skin is attached to the leading edge part, the trailing edge part, spar, and offset parts of the camber morphing wing rib. Conditions were applied so that the leading edge part and the trailing edge part were attached to the skin as the red line shown in Figure 28(a). The red marks in Figure 28(b), the red marks are the fixed joints that connect the skin to the morphing wing rib.

(a)

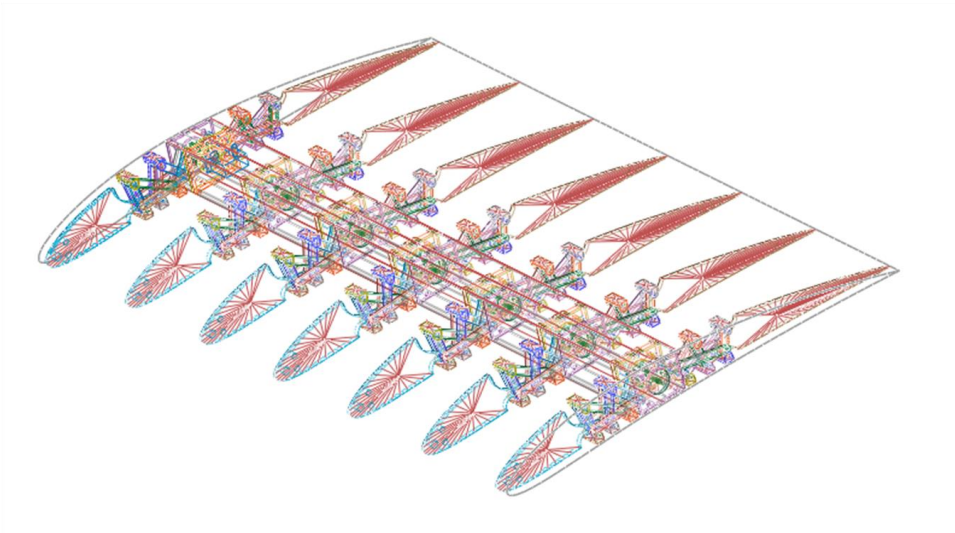

(b)

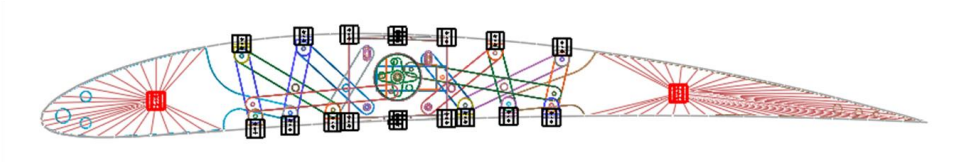

Figure 28. The conditions between the leading edge parts, the trailing edge parts and the skin

Figure 29 shows the spar and skin are bonded at the top and bottom at both ends of edge lines and the center line. Figure 30 shows offset parts and skin.

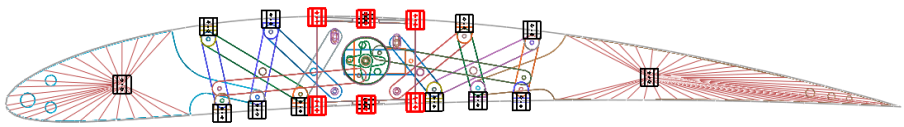

Figure 29. The connection between the spar and the skin

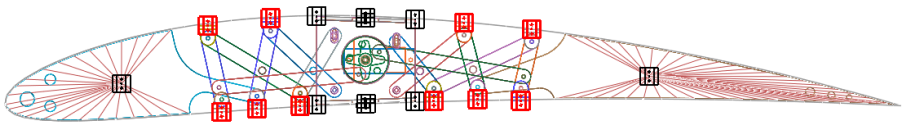

Figure 30. The connection between the offset parts and the skin

Plywood properties were applied to most parts of the morphing wing ribs. All simulations were run for 1 second, and the morphing wing ribs were set to deform the shape within the time.

In Figure 31 and Figure 32, each of the seven ribs shows different target airfoil shapes. The rib closest to the fuselage was set to NACA 2410, and in turn, the camber of the rib was enlarged; thus the farthest rib was set to NACA 8410. In other words, the ribs are deformed to all target airfoils and it can perform as a twist morphing wing. Through the simulation, the von Mises stress distribution of the skin can be seen in Figure 31. In this case, the maximum stress is

obtained as a value of about 4.06MPa. In Figure 32, the von Mises strain distribution of the skin is represented. Through the simulation, the maximum strain of the skin is obtained as 0.935. At this time, there are wrinkles on the skin, which is a phenomenon that occurs because all ribs have different shapes.

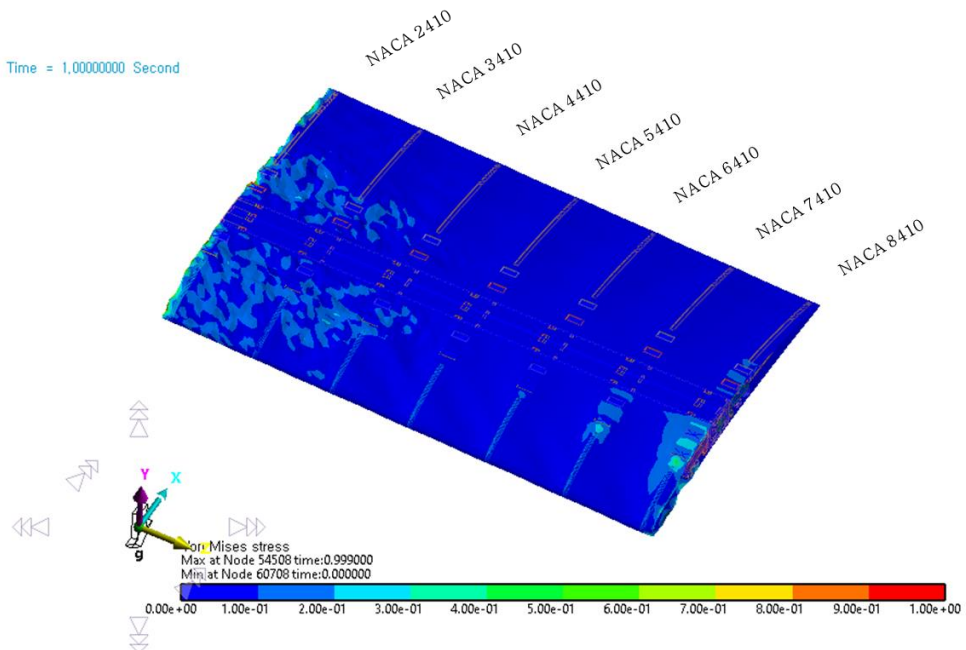

Figure 31. Stress distribution of Skin for all target airfoils

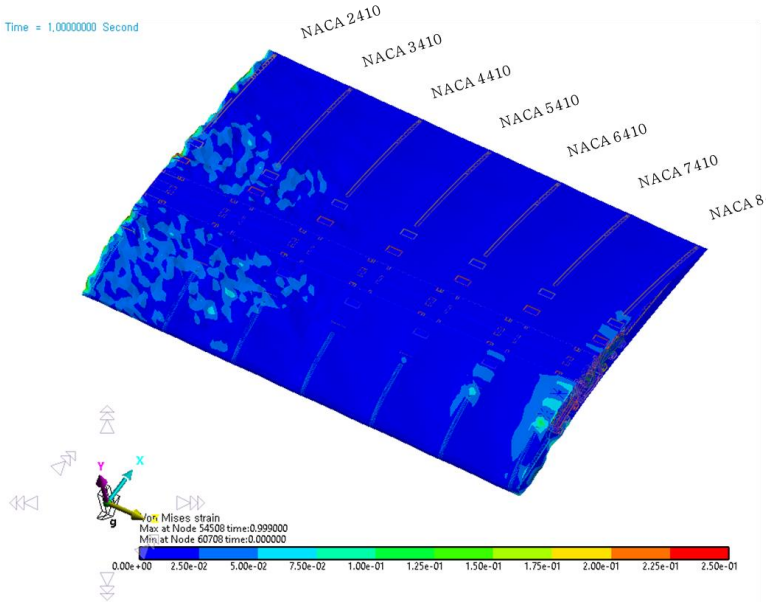

Figure 32. Strain distribution of Skin for all target airfoils

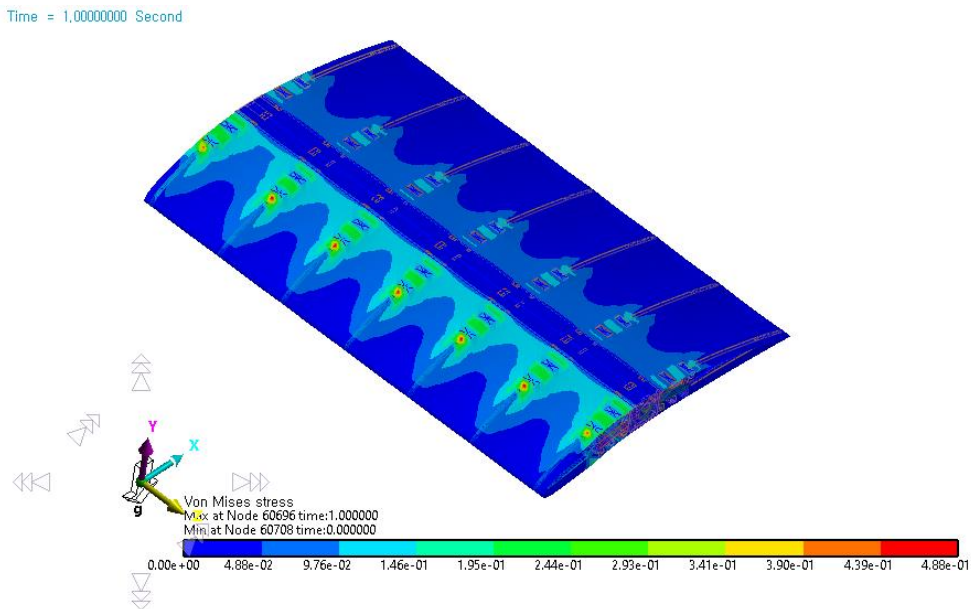

Figure 33. Stress distribution of Skin for NACA 8410

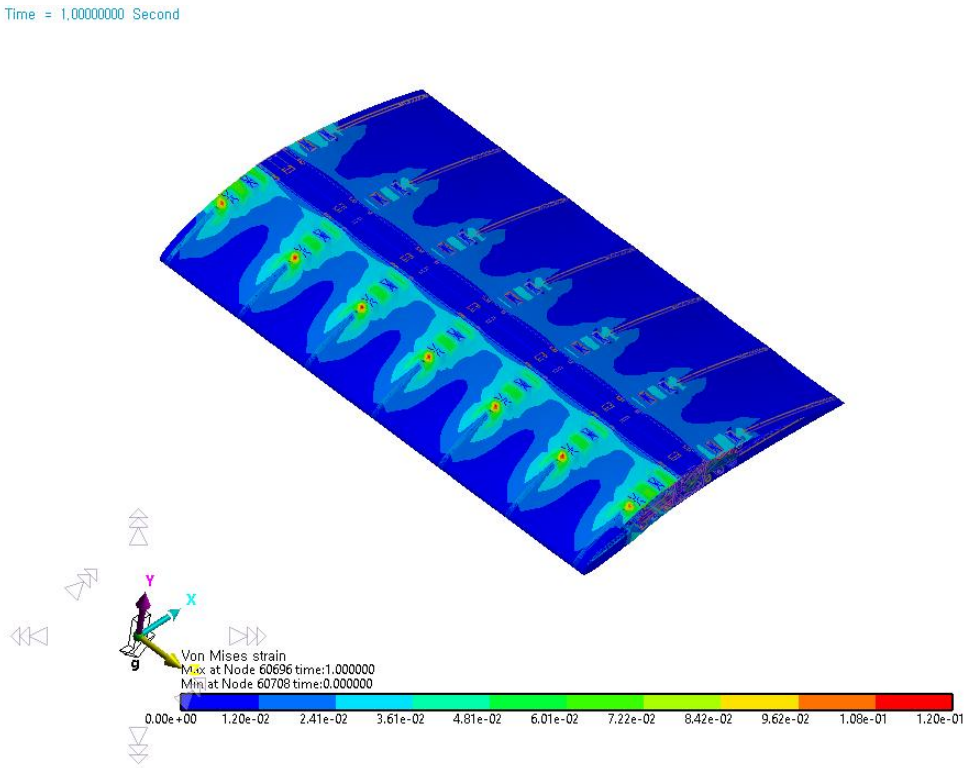

Figure 34. Strain distribution of Skin for NACA 8410

Figure 33 shows the von Mises stress distribution of the skin when all seven ribs are deformed to NACA 8410. When all the ribs are changed to NACA 8410, the ribs have a relatively high-stress level in the leading edge, and the maximum stress on the skin is about 0.49 MPa as shown in Figure 33. Also, in Figure 34, the von Mises strain distribution of the skin for NACA 8410 is represented and has a similar contour to the stress distribution. In this case, the maximum

strain on the skin is obtained as 0.12. The simulation model can predict the stress and strain on the skin at various airfoil configurations during the initial design stage.

5. Manufacturing of Camber Morphing Wing

5.1. Manufacturing and Operability of the Wing Rib

The ribs are made of plywood and fastened using stainless steel 2mm screws. The ribs that make up the wing are made based on the previous model. There are differences between the model of the designed rib and the manufactured rib. Due to the thickness of the plywood, the screws used in the fabrication, the thickness of the ribs and the ribs' placement in the span direction are different from those of the reference model. In Figure 35, among the marked parts, the links at the same position with the leading edge part and trailing edge part are set to be an axis. The other links unmarked in Figure 35 are arranged symmetrically by the axis. In Figure 36 and Figure 37, the number of links is the same as the modeling, but the links are not arranged symmetrically. In Figure 36, the actuator line that connects with the deployable scissor parts and actuator is outward, and in Figure 37 the actuator line is inward. Furthermore, the designed model's links are all modeled with the same thickness. However, the manufactured links have different thicknesses, and a manufactured rib has a thickness of about 32mm. The differences in arrangement

and thickness did not bring any problem for a drive.

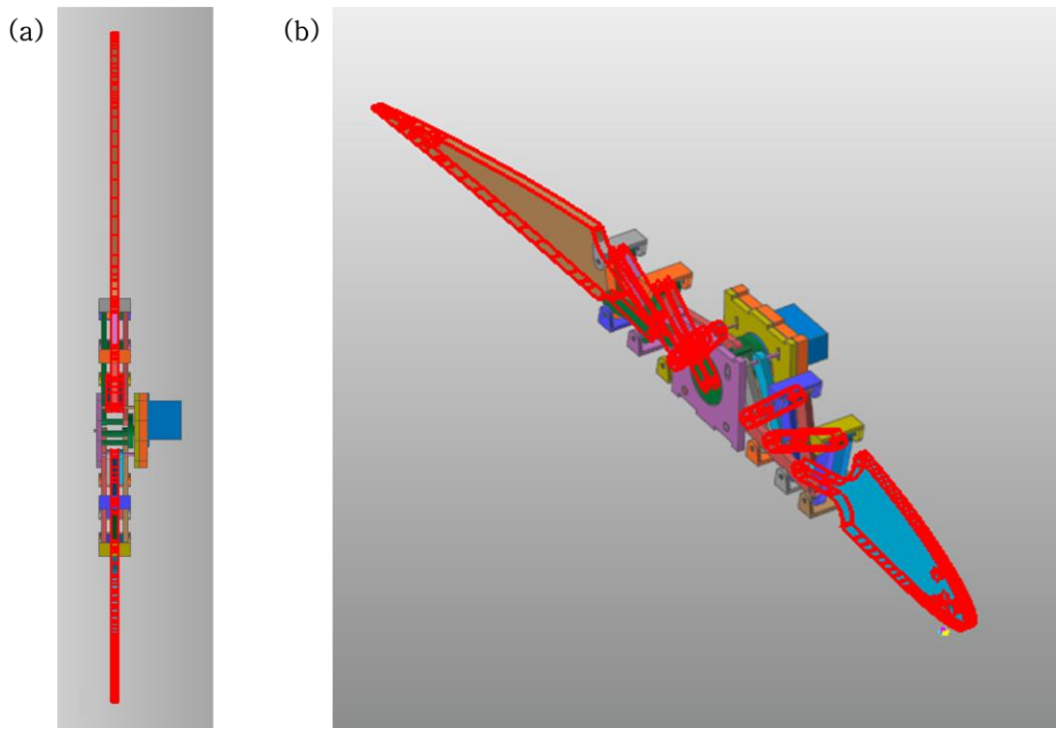

Figure 35. Links having the same position with the leading edge part and the trailing edge part

(a)

(b)

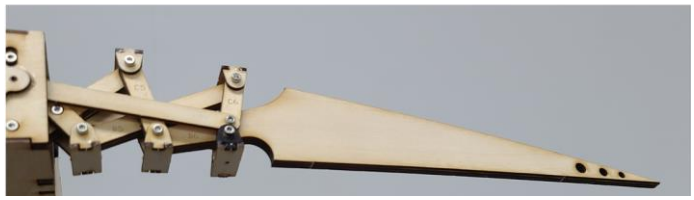

Figure 36. The plane of the rib with the actuator line to outward direction

(a)

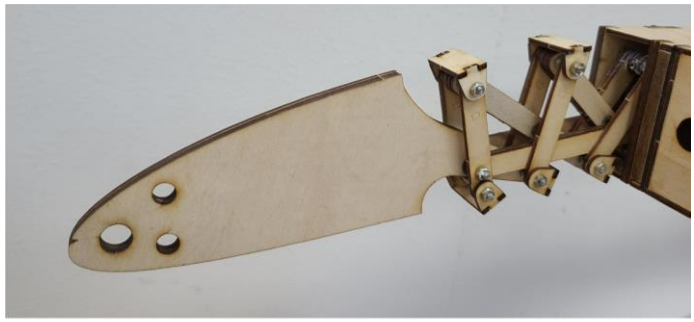

(b)

Figure 37. The plane of the rib with the actuator line to inward direction

As an actuator that supplies the driving force of the rib, a servo motor capable of generating torque of up to 5.3kg/cm^2 ~ 8.5 kg/cm^2 was used, and the weight of the motor is 25g. Figure 38(a) shows NACA 2410, and Figure 38(b) shows NACA 8410.

(a)

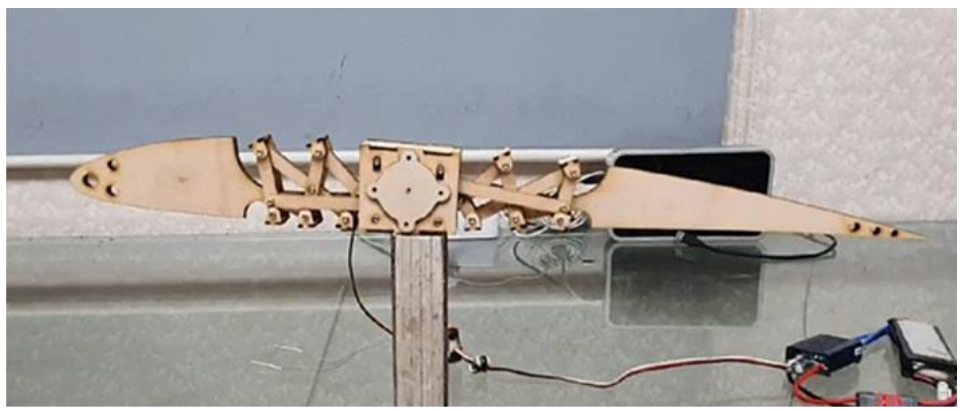

(b)

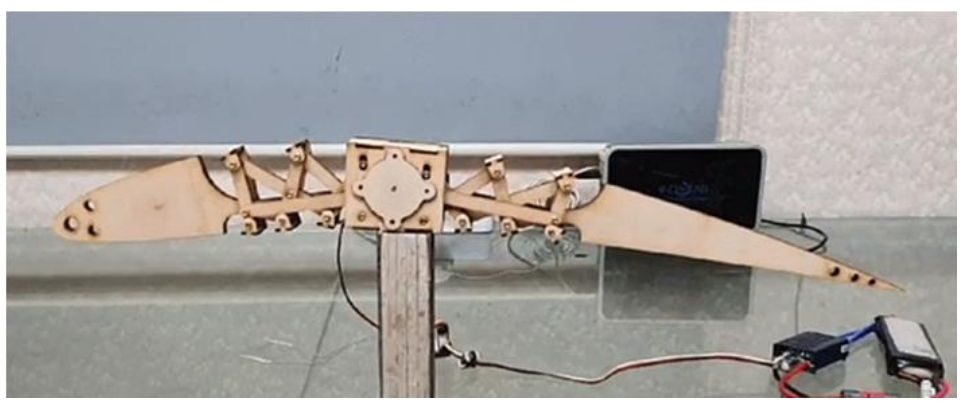

Figure 38. Implementing NACA 2410 and NACA 8410 by manufactured Camber Morphing rib

5.2. Manufacturing and Operability of the Wing

The reference wing model was set with a 1.757m span and 15 ribs. The manufactured wing was made part of the reference modeling and composed of ten ribs. The chord length is 0.5m, which is the same value as the design set but the spacing between the ribs and the rib's thickness are different from the reference of the wing model because of the dimension of screw and wood thickness. As these differences are considered, the span of this wing is about 1.1m. Each rib contains one actuator. Because of the actuator's protrusion closest to the fuselage, only the actuator of this rib was connected in the reverse direction. The wire was lengthened to connect each motor and power source.

Figure 39 shows that all ribs implement NACA 2410, and Figure shows all ribs implement NACA 8410. In Figure 40, the entire wing is twisted by implementing the camber of each rib differently.

Figure 39. Deformed Morphing Wing as NACA 2410

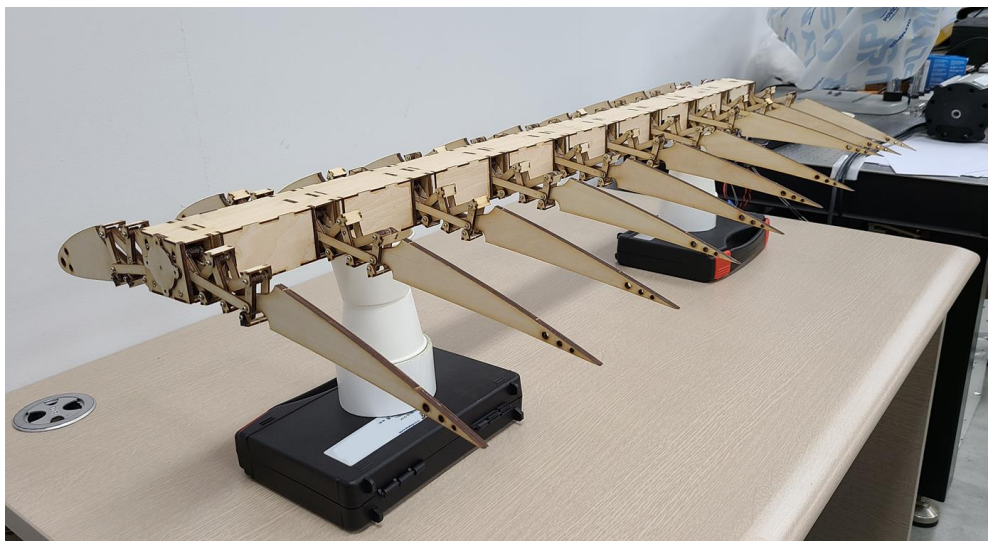

Figure 40. Deformed Morphing Wing as NACA 8410

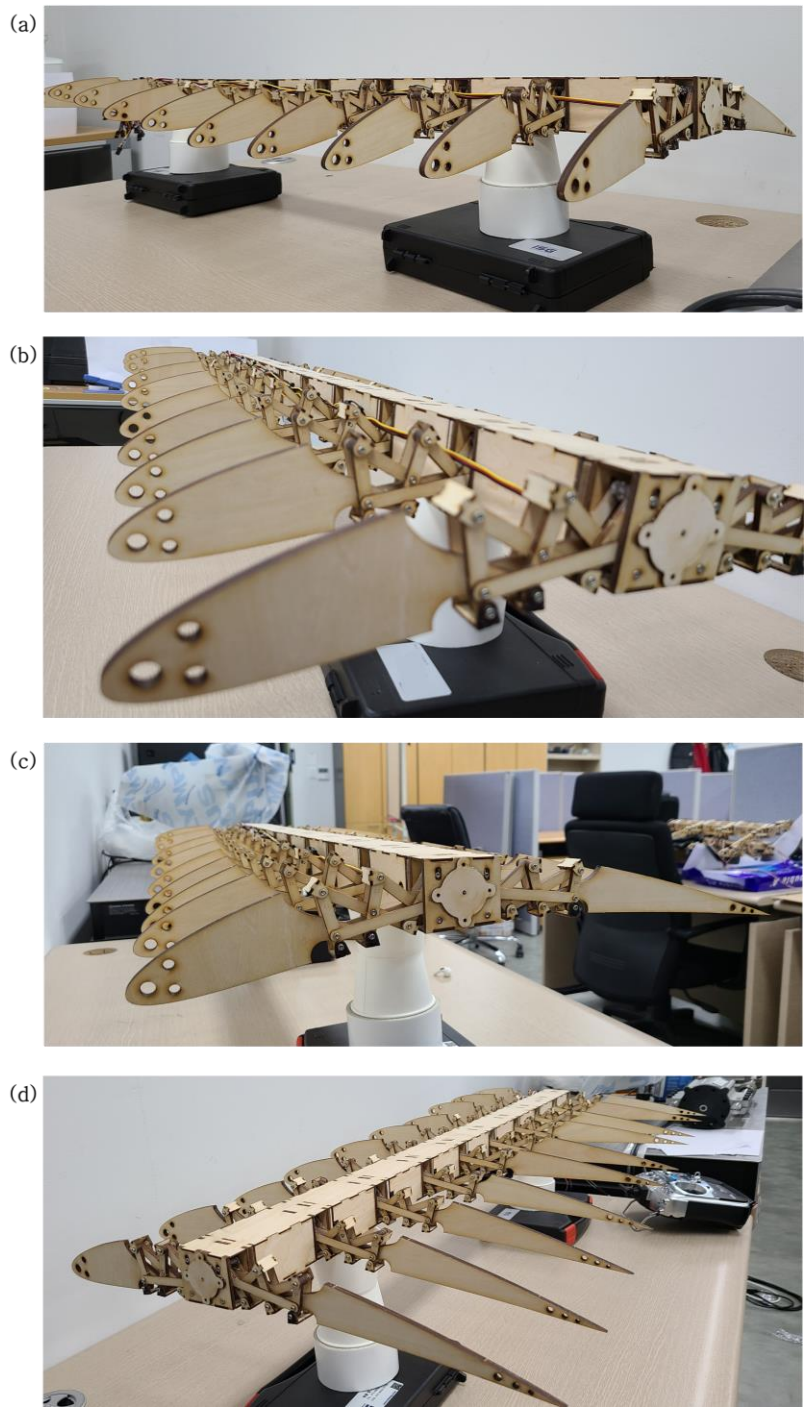

Figure 41. Deformed Morphing Wing as a Twist Morphing Wing

6. Conclusions and future works

6.1. Conclusions

In this thesis, a shape morphing wing with variable camber was designed and manufactured. A new structural mechanism can change the wing's shape while the ribs constituting the camber morphing wing form the airfoil's shape independently. The mechanism was proposed by applying the deployable structure. Therefore, this structure can implement various shapes; the dimensions of the structure were derived through an optimization process. The structure was modeled by applying the obtained dimensions, and the structure was analyzed and manufactured.

The camber morphing wing's internal mechanism applied the deployable scissor structure that can have various curvatures among the deployable structures. The actuator that gives a driving force to the mechanism is connected with the deployable scissor structure. The mathematical model calculated this connection and the mechanism of the entire shape. Using the mathematical model, an optimum design process that reduces the difference in shape from the corresponding target airfoil depending on the actuator's angle

input can be derived. Therefore, each of the ribs independently has one actuator to accurately form the airfoil's shape by the optimum design, and it is possible to perform the task as a twist morphing wing.

Part of the wing was simulated using Recurdyn® V9R3, multi-body dynamic software; it was confirmed that each rib and the entire wing represented the target shapes.

Based on the designed model, a part of the wing was manufactured. The wing is composed of ten ribs and is made of plywood. About its dimension, the span is about 1.1m, the chord length is 0.5m. The actuators of angles were input by a controller, and the ribs constituting the wing formed the target airfoil shapes.

6.2. Future works

In this paper, the ribs performed the optimization process to form the target airfoils. Furthermore, the optimization process will be required for the mechanism design in terms of the weight of the structure, the required power, and the components of the deployable structure, and related research will be conducted later.

In the future, the wind tunnel test will be conducted by the

current camber morphing wing model. Through the wind tunnel test, it is expected that it will be possible to know how aerodynamic efficiency can be improved in a given flight environment.

Reference

[1] S. Barbarino, O. Bilgen, R. M. Ajaj, M. I. Friswell, and D. J. Inman, "A review of morphing aircraft," *J. Intell. Mater. Syst. Struct.*, vol. 22, no. 9, pp. 823–877, 2011.

[2] D. A. Perkins, J. L. Reed, Jr., and E. Havens, "Adaptive wing structures," *Smart Struct. Mater. 2004 Ind. Commer. Appl. Smart Struct. Technol.*, vol. 5388, p. 225, 2004.

[3] J. S. Bae, T. M. Seigler, and D. J. Inman, "Aerodynamic and static aeroelastic characteristics of a variable-span morphing wing," *J. Aircr.*, vol. 42, no. 2, pp. 528–534, 2005.

[4] J. Mestrinho, P. Gamboa, and P. Santos, "Design optimization of a variable-span morphing wing for a small UAV," *Collect. Tech. Pap. - AIAA/ASME/ASCE/AHS/ASC Struct. Struct. Dyn. Mater. Conf.*, no. April, pp. 1–18, 2011.

[5] R. M. Ajaj, M. I. Friswell, E. I. Saavedra Flores, O. Little, and A. T. Isikveren, "Span morphing: A conceptual design study," *Collect. Tech. Pap. - AIAA/ASME/ASCE/AHS/ASC Struct. Struct. Dyn. Mater. Conf.*, no. April, pp. 1–12, 2012.

[6] R. D. Vocke, C. S. Kothera, B. K. S. Woods, and N. M. Wereley, "Development and testing of a span-extending morphing wing," *J. Intell. Mater. Syst. Struct.*, vol. 22, no. 9, pp. 879–890, 2011.

[7] N. Prabhakar, R. J. Prazenica, and S. Gudmundsson, "Dynamic analysis of a variable-span, variable-sweep morphing UAV," *IEEE Aerosp. Conf. Proc.*, vol. 2015-June, 2015.

[8] R. M. Ajaj, M. I. Friswell, M. Bourchak, and W. Harasani, "Span morphing using the GNATSpar wing," *Aerosp. Sci. Technol.*, vol. 53, pp. 38–46, 2016.

[9] R. M. Ajaj *et al.*, “The Zigzag wingbox for a span morphing wing,” *Aerosp. Sci. Technol.*, vol. 28, no. 1, pp. 364–375, 2013.

[10] R. M. Ajaj, E. I. Saavedra Flores, M. I. Friswell, and F. A. D. De la O, “Span Morphing Using the Compliant Spar,” *J. Aerosp. Eng.*, vol. 28, no. 4, p. 04014108, 2015.

[11] D. A. Neal, M. G. Good, C. O. Johnston, H. H. Robertshaw, W. H. Mason, and D. J. Inman, “Design and wind-tunnel analysis of a fully adaptive aircraft configuration,” *Collect. Tech. Pap. - AIAA/ASME/ASCE/AHS/ASC Struct. Struct. Dyn. Mater. Conf.*, vol. 3, no. April, pp. 2387–2395, 2004.

[12] R. Vos, Z. Gürdal, and M. Abdalla, “Mechanism for warp-controlled twist of a morphing wing,” *J. Aircr.*, vol. 47, no. 2, pp. 450–457, 2010.

[13] W. Raither, M. Heymanns, A. Bergamini, and P. Ermanni, “Morphing wing structure with controllable twist based on adaptive bending-twist coupling,” *Smart Mater. Struct.*, vol. 22, no. 6, 2013.

[14] M. Majji, O.K. Rediniotis, and J.L. Junkins, "Design of a morphing wing: modeling and experiments." *AIAA Atmospheric Flight Mechanics Conference and Exhibit*. 2007.

[15] M. Abdulrahim, “Flight performance characteristics of a biologically-inspired morphing aircraft,” *43rd AIAA Aerosp. Sci. Meet. Exhib. - Meet. Pap.*, no. January, pp. 6657–6671, 2005.

[16] V. Alulema, E. Valencia, D. Pillajo, M. Jácome, J. López, and B. Ayala, “Degree of deformation and power consumption of compliant and rigid-linked mechanisms for variable-camber morphing wing uavs,” *AIAA Propuls. Energy 2020 Forum*, no. September, pp. 1–22, 2020.

[17] O. Bilgen, E. I. S. Flores, and M. I. Friswell, “Optimization of surface-actuated piezocomposite variable-camber morphing wings,” *ASME 2011 Conf. Smart Mater. Adapt. Struct. Intell. Syst. SMASIS 2011*,

vol. 1, pp. 315–322, 2011.

[18] O. Bilgen and M. I. Friswell, “Piezoceramic composite actuators for a solid-state variable-camber wing,” *J. Intell. Mater. Syst. Struct.*, vol. 25, no. 7, pp. 806–817, 2014.

[19] A. S. Dale, J. E. Cooper and A. Mosquera, "Adaptive Camber-Morphing Wing using 0-? Honeycomb."*54th AIAA/ASME/ASCE/AHS/ASC Structures, Structural Dynamics, and Materials Conference*. 2013.

[20] J. H. S. Fincham and M. I. Friswell, “Aerodynamic optimisation of a camber morphing aerofoil,” *Aerosp. Sci. Technol.*, vol. 43, pp. 245–255, 2015.

[21] J. J. Joo, C. R. Marks, and L. Zientarski, “Active wing shape reconfiguration using a variable camber compliant wing system,” *ICCM Int. Conf. Compos. Mater.*, vol. 2015-July, no. July, pp. 19–24, 2015.

[22] J. J. Joo, C. R. Marks, L. Zientarski, and A. J. Culler, “Variable Camber Compliant Wing - Design,” no. January, 2015.

[23] C. R. Marks, L. Zientarski, A. Culler, B. Hagen, B. Smyers, and J. J. Joo, “Variable camber compliant wing – wind tunnel testing,” *23rd AIAA/AHS Adapt. Struct. Conf.*, no. January, 2015.

[24] H. Takahashi, T. Yokozeki, and Y. Hirano, “Development of variable camber wing with morphing leading and trailing sections using corrugated structures,” *J. Intell. Mater. Syst. Struct.*, vol. 27, no. 20, pp. 2827–2836, 2016.

[25] B. K. S. Woods, I. Dayyani, and M. I. Friswell, “Fluid/structure-interaction analysis of the fish-bone-active-camber morphing concept,” *J. Aircr.*, vol. 52, no. 1, pp. 307–319, 2015.

[26] B. K. Woods, O. Bilgen, and M. I. Friswell, “Wind tunnel testing of the

fish bone active camber morphing concept," *J. Intell. Mater. Syst. Struct.*, vol. 25, no. 7, pp. 772–785, 2014.

[27] T. Yokozeki, A. Sugiura, and Y. Hirano, "Development and wind tunnel test of variable camber morphing wing," *22nd AIAA/ASME/AHS Adapt. Struct. Conf.*, no. January, pp. 6–13, 2014.

[28] T. Yokozeki, A. Sugiura, and Y. Hirano, "Development of variable camber morphing airfoil using corrugated structure," *J. Aircr.*, vol. 51, no. 3, pp. 1023–1029, 2014.

[29] A. Y. N. Sofla, S. A. Meguid, K. T. Tan, and W. K. Yeo, "Shape morphing of aircraft wing: Status and challenges," *Mater. Des.*, vol. 31, no. 3, pp. 1284–1292, 2010.

[30] H. You, S. Kim, W. Y. Joe, and G. J. Yun, "New concept for aircraft morphing wing skin: Design, modeling, and analysis," *AIAA J.*, vol. 57, no. 5, pp. 1786–1792, 2019.

[31] G. E. Fenci and N. G. R. Currie, "Deployable structures classification: A review," *Int. J. Sp. Struct.*, vol. 32, no. 2, pp. 112–130, 2017.

[32] N. De Temmerman, "Design and analysis of deployable bar structures for mobile architectural applications," *Vrije Univ. Brussel. PhD Diss.*, no. June, p. 314, 2007.

[33] W. M. Sokolowski and S. C. Tan, "Advanced self-deployable structures for space applications," *J. Spacecr. Rockets*, vol. 44, no. 4, pp. 750–754, 2007.

[34] Y. Wang, R. Liu, H. Yang, Q. Cong, and H. Guo, "Design and deployment analysis of modular deployable structure for large antennas," *J. Spacecr. Rockets*, vol. 52, no. 4, pp. 1101–1111, 2015.

[35] R. Zhang, X. Guo, Y. Liu, and J. Leng, "Theoretical analysis and experiments of a space deployable truss structure," *Compos. Struct.*, vol. 112, no. 1, pp. 226–230, 2014.

[36] Y. Akgün, C. J. Gantes, K. E. Kalochairetis, and G. Kiper, "A novel concept of convertible roofs with high transformability consisting of planar scissor-hinge structures," *Eng. Struct.*, vol. 32, no. 9, pp. 2873–2883, 2010.

[37] Y. Akgün, C. J. Gantes, W. Sobek, K. Korkmaz, and K. Kalochairetis, "A novel adaptive spatial scissor-hinge structural mechanism for convertible roofs," *Eng. Struct.*, vol. 33, no. 4, pp. 1365–1376, 2011.

[38] J. S. Zhao, F. Chu, and Z. J. Feng, "The mechanism theory and application of deployable structures based on SLE," *Mech. Mach. Theory*, vol. 44, no. 2, pp. 324–335, 2009.

[39] L. Alegria Mira, A. P. Thrall, and N. De Temmerman, "Deployable scissor arch for transitional shelters," *Autom. Constr.*, vol. 43, pp. 123–131, 2014.

[40] T. Langbecker, "Kinematic analysis of deployable scissor structures," *Int. J. Sp. Struct.*, vol. 14, no. 1, pp. 1–15, 1999.

[41] K. Roovers and N. De Temmerman, "Deployable scissor grids consisting of translational units," *Int. J. Solids Struct.*, vol. 121, pp. 45–61, 2017.

[42] H. J. Qi, K. Joyce, and M. C. Boyce, "Durometer hardness and the stress-strain behavior of elastomeric materials," *Rubber Chem. Technol.*, vol. 76, no. 2, pp. 419–435, 2003.

[43] R. F. Gibson, *Principles of Composite Material Mechanics*. CRC Press/Taylor & Francis Group, LLC, 2016.

국문초록

전개형 시저스 구조를 이용한 가변 캠버 모핑 날개 설계, 해석 및 제작

최 이 령
항공우주공학과
서울대학교 대학원

형상 가변익은 형상이 변하는 날개를 의미한다. 본 학위논문에서는 형상 가변익 중에서도 캠버를 변형시키는 가변익을 설계하고, 이에 적용되는 스킨을 해석하였으며, 설계 모델을 기반으로 날개를 제작하였다. 캠버 가변익은 일정한 시위선 길이를 가지고 다양한 캠버를 갖는 에어포일 형상들을 만족하도록 설계되었다. 목표 에어포일 형상들은 4자리 NACA 에어포일 형상들로 설정하였으며, 날개를 구성하는 각각 리브가 독립적으로 형상을 구현함으로써 비틀림 날개로써도 임무를 수행할 수 있도록 설계되었다.

캠버 가변익을 구성하는 리브의 구조, 즉 리브의 내부 메커니즘은 새롭게 고안되었으며, 이 메커니즘에는 전개형 구조 중 다양한 곡률을

구현할 수 있는 전개형 시저스 구조를 이용하였다. 전개형 시저스 구조를 내부 메커니즘에 적용할 수 있도록 모델링을 하기 위해 수학적 모델을 만들었으며, 이 수학적 모델은 입력 변수로 설정된 각도에 따라 형상이 결정된다. 이 수학적 모델은 최적화 설계 과정에 적용되었고 최적화 과정을 통해 내부 메커니즘이 만드는 형상과 목표 에어포일 형상들 간의 차이를 줄일 수 있게 되어, 목표 에어포일 형상들을 구현하게 된다. 내부 메커니즘의 형상을 변형시키기 위해서는 구동력이 필요하기 때문에, 전개형 구조로 구성된 모델과 구조물에 구동력을 부여하는 작동기와의 연결성을 부여하기 위한 모델링 과정을 수행하였고 작동기에 목표 형상에 대한 각도가 입력되면 그에 상응하는 형상이 구현된다. 완성된 모델을 다물체 동역학 소프트웨어 Recurdyn® V9R3으로 시뮬레이션 하였고, 목표 형상들을 매우 근사하게 구현함을 확인하였다.

캠버 모핑윙의 구조는 움직이며 형상이 달라지기 때문에, 날개를 덮는 스킨은 구조 형상 변화에 따라 늘어날 수 있을 만큼 유연해야 한다. 또한 스킨은 방향에 따라 다른 특성을 가져야 하므로 복합재를 적용하여, 이에 따른 스킨의 거동에 대해 다물체 동역학 소프트웨어 Recurdyn® V9R3를 이용하여 해석을 수행하였다.

위 과정을 토대로 설계한 모델에 대해 제작을 수행하였다. 스팬은

약 1.1m, 시위선 길이는 0.5m로, 재료는 합판을 사용하여 제작이 수행되었다. 제작된 날개는 10개의 리브로 구성되었으며, 각각의 리브마다 하나의 작동기가 작동하게 된다. 따라서 각각의 리브는 독립적으로 구동되어 서로 다른 형상을 나타낼 수 있으며, 목표 에어포일 형상들을 구현할 수 있다.

Keywords : 가변익, 전개형 구조, 최적 설계 , 캠버

Student Number : 2019-26125